ORKUSTOFNUN
NATIONAL ENERGY AUTHORITY

THE UNITED NATIONS UNIVERSITY

LECTURES ON GEOCHEMICAL INTERPRETATION OF HYDROTHERMAL WATERS

Robert O. Fournier

UNU Geothermal Training Programme
Reykjavík, Iceland
Report 10, 1989

Report 10, 1989

LECTURES ON GEOCHEMICAL INTERPRETATION OF HYDROTHERMAL WATERS

Publication of the
UNU Geothermal Training Programme
National Energy Authority
Grensasvegur 9
108 Reykjavik
Iceland

Address of the author:
U.S. Geological Survey
Menlo Park
California 94025
U.S.A.

PREFACE

Since the foundation of the UNU Geothermal Training Programme in Iceland in 1979, it has been customary to invite annually one geothermal expert to come to Iceland as a UNU Visiting Lecturer. The UNU Visiting Lecturers have been in residence in Reykjavik from one to eight weeks. They have given a series of lectures on their speciality and held discussion sessions with the UNU Fellows attending the Training Programme. The lectures of the UNU Visiting Lecturers have also been open to the geothermal community in Iceland, and have always been very well attended. It is the good fortune of the UNU Geothermal Training Programme that so many distinguished geothermal specialists with an international reputation have found time to visit us. Following is a list of the UNU Visiting Lecturers during 1979-1988:

1979	Donald E. White	United States
1980	Christopher Armstead	United Kingdom
1981	Derek H. Freeston	New Zealand
1982	Stanley H. Ward	United States
1983	Patrick Browne	New Zealand
1984	Enrico Barbier	Italy
1985	Bernardo S. Tolentino	Philippines
1986	C. Russel James	New Zealand
1987	Robert Harrison	United Kingdom
1988	Robert O. Fournier	United States

The UNU Visiting Lecturer of 1988, Dr. Robert O. Fournier, has for about two decades been one of the leading authorities in the world on the interpretation of the chemical composition of hydrothermal waters. It is a great honour for the UNU Geothermal Training Programme to publish here the text of the lectures that he gave in Reykjavik in the fall of 1988. We are very grateful for the contribution of Dr. Fournier to the Training Programme and its efforts to assist scientists and engineers in the developing countries to have access to the most up to date methods for the interpretation of geothermal data.

Ingvar Birgir Fridleifsson,
Director,
United Nations University
Geothermal Training Programme.

CONTENTS

CARBONATE TRANSPORT AND DEPOSITION IN HYDROTHERMAL SYSTEMS

Robert O. Fournier
U.S. Geological Survey, Menlo Park, California 94025 U.S.A.

INTRODUCTION

The alkali carbonates, Na, K, and Li, are relatively soluble at all temperatures and generally precipitate only where there is extreme evaporation. In contrast, the alkaline earth carbonates, Ca, Mg, Sr, and Ba, are moderately to sparingly soluble and commonly precipitate in hydrothermal systems. Calcite is by far the most abundant and important carbonate found in hydrothermal systems, and more solubility data are available for it than for any of the other carbonates. In natural hydrothermal solutions many dissolved constituents and a variety of chemical reactions involving solids, liquids, and gases influence the dissolution and deposition of calcite. In particular, its solubility is strongly influenced by pH, the partial pressure of carbon dioxide, P_{CO2}, temperature, and the presence of other dissolved salts. The situation is particularly complex when boiling occurs. Sophisticated computer programs, such as the WATCH programs (Svararsson, 1981), are the best way to handle these complex reactions. However, all too frequently such programs are employed with little regard or appreciation for the factors that influence the results of the computations. It is the intent of this presentation to highlight the factors that control the solution and deposition of carbonate in geothermal systems, and to show that it is possible to make good estimates of the likely magnitude of calcite transport and deposition in natural waters using hand-held, programmable calculators. These procedures are very useful even though a few simplifying assumptions are required, and only the most important dissolved species are included. The ensuing discussion follows the general procedures presented in Henley et al. (1984).

CO_2 DISSOLVED IN AQUEOUS SOLUTIONS

According to Henry's Law, the amount of CO_2 that will dissolve in a liquid is given by the relationship,

$$f_{CO2} = K_H X \ , \qquad (1)$$

where f_{CO2} is the fugacity of carbon dioxide, X is the mole fraction of carbon dioxide dissolved in the liquid phase, and K_H is the Henry's Law constant. Actually, K_H is different at different temperatures and for different liquid salinities (Fig. 1). Because fugacity coefficients for carbon dioxide in aqueous solutions at temperatures below about 330°C are near unity, f_{CO2} in equation (1) can be replaced by the partial pressure of carbon dioxide, P_{CO2}, with little error. An equation giving P_{CO2} in geothermal reservoirs as a function of temperature has been published by Arnorsson (1985) and reproduced as equation (m) in Table 1. An equation expressing Henry's Law coefficient for the system carbon dioxide-water as a function of temperature is given in Table 1, equation (a). The constants used in the equations of Table 1 are given in Table 2. Values of the Henry's Law coefficient for the system CO_2-H_2O at selected temperatures are given in Table 3. Adding salt to the system CO_2-H_2O increases the Henry's Law coefficient and decreases the solubility of carbon dioxide in the solution (Fig. 1). This decrease in solubility of a gas in a saline solution compared to the solubility in pure water is called "salting-out." Salting-out coefficients for carbon dioxide in sodium chloride solutions generally are of the Steschenow type,

$$k = \frac{1}{\underline{m}} \log (K_H/K°_H) \ , \qquad (2)$$

where k is the salting-out coefficient, $\underline{m}$ is the molality of NaCl, and $K°_H$ and K_H are respectively the Henry's Law coefficients for pure water as solvent and for the saline solution (Ellis and Golding, 1963). Approximate salting-out coefficients can be obtained from equation (b) in Table 1 and at selected temperatures from Table 3.

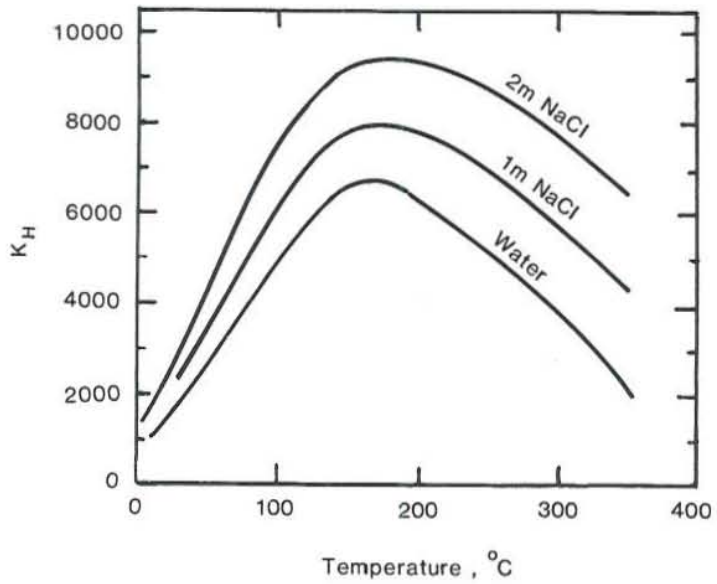

FIGURE 1. Values of Henry's Law constant, K_H, for the solution of carbon dioxide in water and sodium chloride solutions. (Redrawn from Ellis and Golding, 1963).

Some dissolved carbon dioxide reacts with water (hydrates) to form carbonic acid,

$$CO_{2(dissolved)} + H_2O = H_2CO_3 \ , \tag{3}$$

and some of the carbonic acid, in turn, dissociates according to the reactions,

$$H_2CO_3 = HCO_3^- + H^+, \tag{4}$$

$$K_1 = \frac{[HCO_3^-]\ [H^+]}{[H_2CO_3]} \ , \tag{5}$$

$$HCO_3^- = CO_3^= + H^+, \tag{6}$$

$$K_2 = \frac{[CO_3^=]\ [H^+]}{[HCO_3^-]} \ , \tag{7}$$

where square brackets indicate activities of the enclosed species, and K_1 and K_2 are respectively the first and second dissociation constants of

carbonic acid (Table 3). Equations (c) and (d) in Table 1 express the temperature dependence of K_1 and K_2. The reaction shown by equation (3) takes place relatively slowly, while the reaction shown by equation (4) is almost instantaneous. This information will be of use later when the consequences of boiling are discussed.

By tradition, a distinction is not made between aqueous CO_2 and H_2CO_3, and total dissolved CO_2 is reported as H_2CO_3. A net reaction is generally written

$$CO_{2(gas)} + H_2O = H_2CO_3 \ , \tag{8}$$

$$K_0 = \frac{[H_2CO_3]}{f_{CO2}[H_2O]} \ , \tag{9}$$

where K_0 is the equilibrium constant for the reaction shown by equation (8). Values of K_0 at temperatures ranging from 100° to 300°C (Table 3) can be calculated using equation (e) in Table 1. The $[H_2CO_3]$ term in equations (5) and (9) includes the activity of dissolved, nonhydrated CO_2. Aqueous, nonhydrated CO_2 is more abundant than H_2CO_3 in most hydrothermal solutions. Also, H_2CO_3 is less ionized at high temperatures compared to low temperatures (values of K_1 range from about $10^{-6.57}$ at 0°C to about $10^{-8.29}$ at 300°C). Therefore, as a hydrothermal solution cools, bicarbonate dissociates (equation 4), liberating hydrogen ions that attack the minerals in the wall rock. Hydrolysis reactions involving feldspars generally buffer the pH at near neutral to slightly acidic conditions and cooling solutions become richer in cations (Na at higher temperatures and Ca at lower temperatures) as hydrogen ions are consumed by the formation of micas or clays.

Where boiling occurs, generally as a result of decreasing hydrostatic pressure exerted upon an ascending hydrothermal solution, CO_2 is strongly partitioned into the gas (steam-rich) phase. The total gas pressure is equal to the sum of the partial pressures of all the constituent gases, and these partial pressures are proportional to the respective mole fractions. By Raoult's Law, for a mixture of two components that exhibit ideal behavior (may be closely approximated when the components are similar in molecular structure or when one of the components is present in great excess),

$$P_{Total} = P_a + P_b = P^*_a X_a + P^*_b X_b = P^*_a X_a + P^*_b (1-X_a) \ , \tag{10}$$

where P^*_a and P^*_b are the vapor pressures of pure components A and B respectively at the given temperature, and X_a and X_b are the respective mole fractions of A and B in the mixture.

When boiling is first initiated the ratio of CO_2 to water in the gas phase tends to be relatively large because most of the carbon dioxide initially dissolved in the liquid exsolves quickly into the gas phase while only a small amount of water changes to steam. With continued boiling, the mole fraction of CO_2 in the gas phase steadily decreases because little additional CO_2 is available to partition into the gas phase while the fraction of water that is converted to steam increases at a relatively constant rate. As the temperature of the ascending gas-water mixture decreases, the volume of the gas phase increases due to the decrease in hydrostatic load. The net effect is a drastic decrease in the partial pressure of CO_2 as a boiling fluid ascends toward the earth's surface.

For relatively dilute systems and low initial dissolved gas concentrations, a distribution coefficient, B, is defined as the concentration of gas in the vapor divided by the concentration of gas in the liquid. The temperature dependence of B for carbon dioxide in dilute aqueous solutions is given by

$$\log B = 4.7593 - 0.01092t \ , \tag{11}$$

where t is temperature in degrees Celsius. Equation (11) is valid from 100° to 340°C. The following equation can be used to calculate the concentration of CO_2 remaining in the liquid phase (C_l) for the situation in which all the evolved gas remains in contact with a boiling fluid during adiabatic decompression (single-step steam separation).

$$C_l = \frac{C_o}{1 + y(B - 1)} \ , \tag{12}$$

where C_o is the initial concentration of dissolved CO_2 before boiling, B is the distribution coefficient, and y is the fraction of separated steam. The corresponding equation that gives the concentration of CO_2 in the coexisting steam (C_v) is

$$C_v = \frac{C_o}{(1/B)(1 - y) + y} \ . \tag{13}$$

Values of y are generally calculated using enthalpy data for pure boiling water and the relationship,

$$y = \frac{H_o - H_L}{H_G - H_L}, \qquad (14)$$

where H_o is the enthalpy of the initial liquid prior to boiling, and H_L and H_G are the enthalpies of coexisting liquid water and steam after boiling (Table 3). Enthalpies of liquid water and steam are generally obtained from steam tables or they can be calculated using equations (f) and (g) in Table 1. Equation (13), however, yields values of y that are slightly in error because the enthalpy of steam containing CO_2 is different than the enthalpy of pure steam. Other factors also may cause the calculated concentration of CO_2 in the liquid and steam fractions of a boiling solution to be in error. Assumptions implicit in the use of equations (12) and (13) are that dissolved CO_2 does not become supersaturated in the liquid phase as pressure is released, and that little or no H_2CO_3 converts to HCO_3^- as the boiling solution cools. The rapid transfer of most of the dissolved CO_2 into the steam fraction at an early stage of boiling and the relatively slow conversion of dissolved CO_2 to H_2CO_3 (previously discussed) will tend to limit the amount of HCO_3^- that can form, but some nonequilibrium partitioning of CO_2 between the liquid and gas phase is likely, particularly when the first boiling is initiated at a temperature below about 200°C. Another factor that must be considered is physical removal of the steam fraction from contact with the residual liquid as the boiling process proceeds. Compared to single-step steam separation, multistep and continuous steam separation result in much lower concentrations of CO_2 in the last liquid and steam fractions that are in contact. Henley et al. (1984) present methods and equations for dealing with multistep and continuous steam separation. Figure 2 shows values of C_1/C_o for single-step steam separation for a variety of initial and final temperatures, calculated using equations (12) and (14).

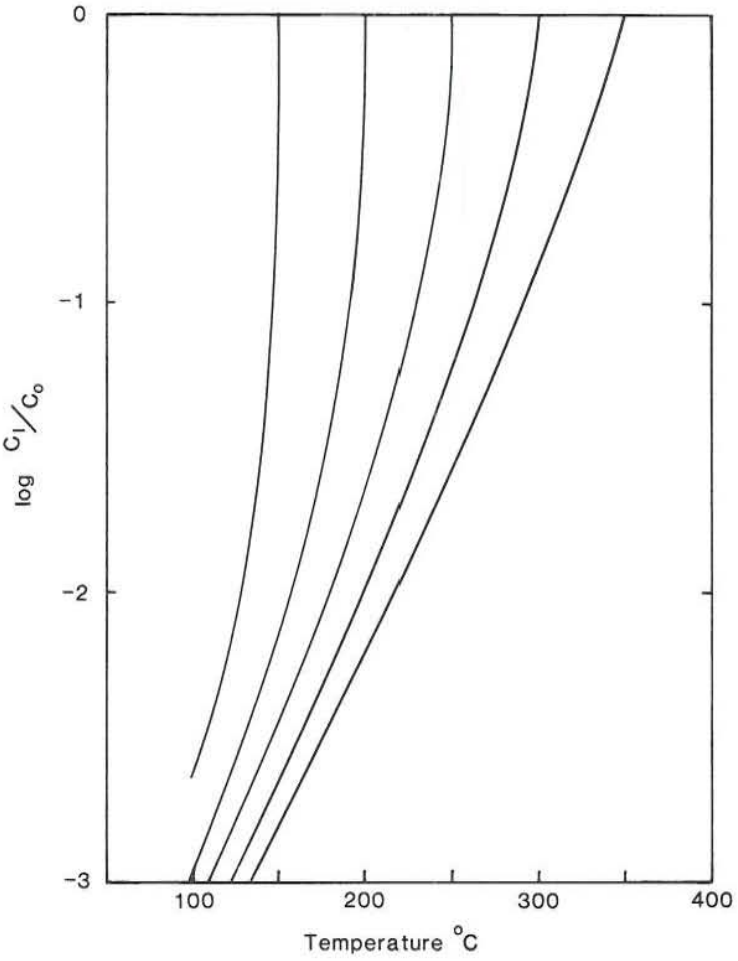

FIGURE 2. The ratio of CO_2 remaining in the residual liquid (C_1) after single-step steam separation at various temperatures to CO_2 in the initial liquid (C_o) before boiling.

THE SOLUBILITY OF CALCITE IN AQUEOUS SOLUTIONS

At a given partial pressure of CO_2, the solubility of calcite decreases with increasing temperature (Fig. 3). Adding NaCl to the solution increases the solubility of calcite (Fig. 4). At any given temperature the solubility of calcite in solutions in equilibrium with a vapor phase increases with increasing CO_2 pressure until $\underline{m}\ CO_2 \simeq 1$ mole/kg. In solutions held at a constant total pressure, the solubility increases with increasing CO_2 concentration until $\underline{m}\ CO_2 \simeq 1$ mole/kg and then decreases at higher CO_2 concentrations.

The simplest equation representing the reaction by which calcite dissolves in aqueous solutions can be written as

$$CaCO_3 = Ca^{++} + CO_3^{=} \quad , \tag{15}$$

and the equilibrium constant (K_c) for reaction (15) is

$$K_c = \frac{[Ca^{++}]\ [CO_3^{=}]}{[CaCO_3]} \quad . \tag{16}$$

Equation (16) is useful mainly for testing whether a solution of given composition is unsaturated, saturated, or supersaturated in respect to calcite. Values of K_c in the temperature range 100° to 300°C (Table 3) can be calculated using equation (h) in Table 1. Because very little $CO_3^{=}$ is present in most natural hydrothermal solutions, the solubility of calcite is commonly expressed in terms of reactions involving H^+, HCO_3^-, and f_{CO2} using equations (5), (7), (9), and (16).

$$CaCO_3 + H^+ = Ca^{++} + HCO_3^- \quad , \tag{17}$$

$$\frac{K_c}{K_2} = \frac{[Ca^{++}]\ [HCO_3^-]}{[H^+]\ \ [CaCO_3]} \quad , \tag{18}$$

$$CaCO_3 + 2H^+ = Ca^{++} + H_2O + CO_2 \quad , \tag{19}$$

$$\frac{K_c}{K_1K_2K_0} = \frac{[Ca^{++}]\ [H_2O]\ f_{CO2}}{[H^+]^2\ [CaCO_3]} \quad , \tag{20}$$

$$CaCO_3 + CO_2 + H_2O = Ca^{++} + 2HCO_3^- \quad , \tag{21}$$

$$\frac{K_cK_1K_0}{K_2} = \frac{[Ca^{++}\ [HCO_3^-]^2}{[H_2O]\ f_{CO2}\ [CaCO_3]} \quad . \tag{22}$$

In equations (16), (18), (20), and (22), the activity of calcite is unity if there is no significant substitution of other cations for calcium in solid solution, such as Mg, Fe, or Mn.

In order to evaluate equations (16-22), activities of the indicated aqueous species must be used. In dilute solutions, activities of dissolved constituents are about equal to the corresponding molalities. In saline solutions, however, the molality of each species i ($\underline{m}_i$) must be multiplied by its activity coefficient (γ_i) to obtain the activity ($a_i = \underline{m}_i \gamma_i$). Activity coefficients for solutions with ionic strengths less than about 2 molal can be calculated using an extended form of the Debye-Huckel equation,

$$- \log \gamma_i = \frac{A z_i^{\,2} I^{1/2}}{1 + \mathring{a}_i B I^{1/2}} + bI \ , \qquad (23)$$

where z_i is the ionic charge, I the ionic strength, and A, B, $\mathring{a}_i$ and b are constants. However, A and B vary with temperature. Their values from 100° to 350°C, in 25°C increments, are given in Table 3. The coefficients A and B also can be calculated to three decimal places using equations (i) and (j) in Table 1. The ionic strength is defined as

$$I = 1/2 \ \ \underline{m}_i z_i^{\,2} \ . \qquad (24)$$

For most hydrothermal waters I is approximately equal to the sum of $\underline{m}_{Na^+}$ and $\underline{m}_{K^+}$. Values of $\mathring{a}_i$ and z_i are listed in Table 4. Up to 250°C, b has values in the range 0.03 to 0.05 when concentrations are up to 3 molal.

From a consideration of the cation-anion charge balance that must be maintained in all solutions (and neglecting effects of oxidation-reduction reactions and pH-dependent ions that are likely to be present only in very small amounts in most natural hydrothermal solutions, such as $CO_3^{=}$, $H_2SiO_4^{=}$, and OH^-) a constant, δ, can be defined that is independent of temperature and equal to the sum of the principal pH-dependent ions,

$$\delta = [\underline{m}_{HCO3^-} + \underline{m}_{H3SiO4^-} + \underline{m}_{H2BO3^-}] - [\underline{m}_{NH4^+} + \underline{m}_{H^+}] \ . \qquad (25)$$

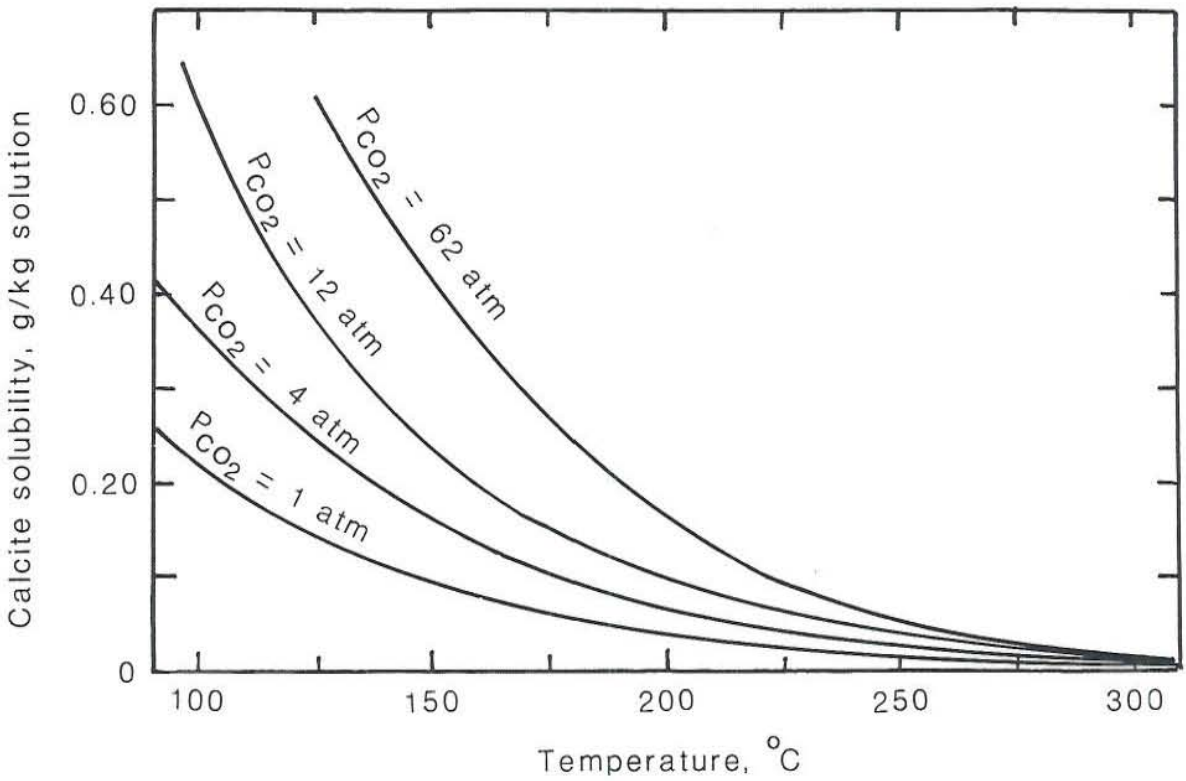

FIGURE 3. The solubility of calcite in water up to 300°C at various partial pressures of carbon dioxide. (Redrawn from Ellis, 1959).

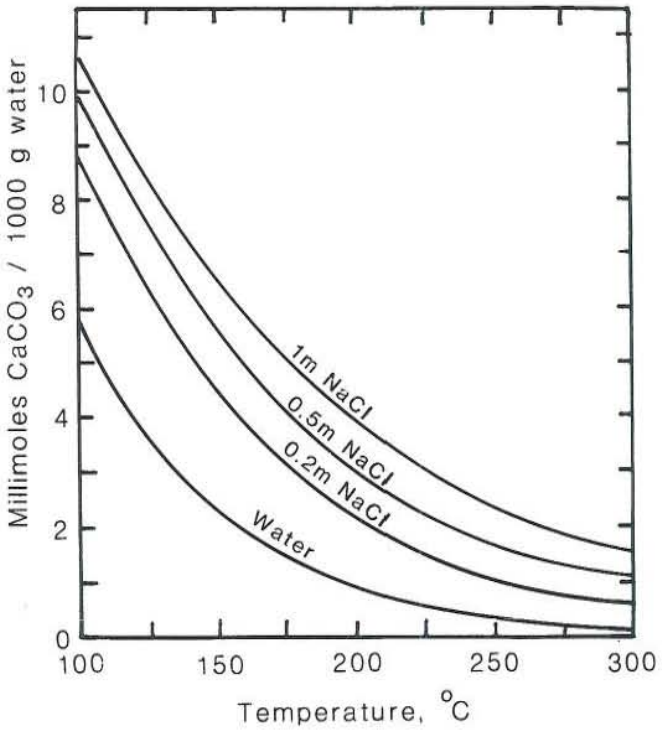

FIGURE 4. The solubility of calcite in water and sodium chloride solutions at a carbon dioxide pressure of 12 atmospheres (12.2 bars). (Redrawn from Ellis, 1963).

The concentrations of the ionic species indicated in equation (25) can be calculated using the following relationships, where K_1 is the first dissociation constant for each of the respective weak acids.

$$\underline{m}_{HCO3^-} = \frac{\underline{m}_{CO2(total)}}{\left(\frac{[H^+]\ \gamma_{HCO3^-}}{K_1}\right) + 1}, \tag{26}$$

$$\underline{m}_{H3SiO4^-} = \frac{\underline{m}_{SiO2(total)}}{\left(\frac{[H^+]\ \gamma_{H3SiO4^-}}{K_1}\right) + 1}, \tag{27}$$

$$\underline{m}_{H2BO3^-} = \frac{\underline{m}_{B(total)}}{\left(\frac{[H^+]\ \gamma_{H2BO3^-}}{K_1}\right) + 1}, \tag{28}$$

$$\underline{m}_{NH4^+} = \frac{\underline{m}_{NH3(total)}}{\left(\frac{K_1\ \gamma_{NH4^+}}{[H^+]}\right) + 1}. \tag{29}$$

If the pH, ionic strength, and chemical composition (particularly total dissolved carbon, silica, boron, and ammonia) of a solution are known at a given temperature, equations (25-29) can be used to estimate the indicated species concentrations at any other temperature up to the limit of the available thermodynamic data (now about 300-350°C). Note, however, that equations (25-29) do not take account of changing concentrations and partitioning of constituents between the liquid and gas phase during boiling.

For adiabatic boiling resulting from decompression, the value of δ changes as a function of the fraction of steam (y) that forms

$$\delta_{(\text{before boiling})} = (1 - y)\delta_{(\text{after boiling})}. \tag{30}$$

The effect of partitioning of CO_2 between liquid and gas can be accounted for by using the relationship,

$$A_o = \frac{n_{CO2,l}\ n_{H2O,v}}{n_{CO2,v}\ n_{H2O,l}}\ , \tag{31}$$

where n_l and n_v are the number of moles of the indicated species in the liquid and gas phases, respectively. A_o for dilute solutions also can be calculated using equation (k) in Table 1. Rearranging equation (31) and substituting n_{H2CO3} for $n_{CO2,l}$, and $y/(1-y)$ for $n_{H2O,v}/n_{H2O,l}$,

$$n_{CO2,v} = \frac{n_{H2CO3}}{A_o}\ \frac{y}{(1 - y)}\ . \tag{32}$$

For one-step steam separation without carbonate precipitation (supersaturation allowed in the calculation) the total number of moles of CO_2-bearing species remains constant during the boiling process, even though CO_2 partitions between the gas and liquid phases,

$$n_{CO2(total)} = n_{H2CO3} + n_{CO2(gas)} + n_{HCO3^-} + n_{CO3^=}\ . \tag{33}$$

The concentration of $CO_3^=$ in equation (33) cannot be neglected when solutions boil because the pH may increase significantly. Combining equations (32) and (33),

$$n_{CO2(total)} = n_{H2CO3} + \left(\frac{n_{H2CO3}}{A_o}\ \frac{y}{(1 - y)}\right) + n_{HCO3^-} + n_{CO3^=}\ , \tag{34}$$

and dividing equation (34) by n_{HCO3^-},

$$\frac{n_{CO2(total)}}{n_{HCO3^-}} = \frac{n_{H2CO3}}{n_{HCO3^-}}\ \left(1 + \frac{y}{A_o(1 - y)}\right) + 1\ + \left(\frac{n_{CO3^=}}{n_{HCO3^-}}\right). \tag{35}$$

Equation (35) is expressed in terms of mole ratios, so molal concentration units can be substituted for the number of moles of the given species in the liquid fraction. Combining equations (5), (7), and (35), multiplying molalities by activity coefficients to obtain activities where required, and rearranging gives

$$m_{HCO3^-} = \frac{m_{CO2(total)}}{\left(\frac{[H^+]\ \gamma_{HCO3^-}}{K_1}\right)\left(1 + \frac{y}{A_o(1 - y)}\right) + 1\ + \left(\frac{K_2\ \gamma_{HCO3^-}}{[H^+]\ \gamma_{CO3^=}}\right)}\ . \tag{36}$$

Account can be taken of the partitioning of other volatile constituents in a similar manner. The resulting equations can be used to estimate by iteration the pH and distribution of pH-dependent species at given temperatures for boiling conditions. The equations and procedures are cumbersome using a hand-held calculator, but are easily dealt with using table-top micro or personal computers.

Where cooling occurs adiabatically (generally too quickly for solution-mineral reactions involving silicates to buffer pH) the pH of the residual liquid usually rises as a result of partitioning of CO_2 and other acid-forming gases into the steam phase and calcite commonly precipitates in spite of the decreasing temperature. Arnorsson (1978) calculated the amount and location of calcite deposition in geothermal wells in Iceland where thermal waters flash to steam during production of the resource. The results of his calculations, showing the degree of supersaturation with respect to calcite that occurs during single-step adiabatic flashing (boiling) in the wells, are shown in Figure 5 (supersaturated solutions that plot below the thick solid line). Figure 6 shows calculated changes in pH that accompany single-step adiabatic flashing of natural thermal waters in these wells.

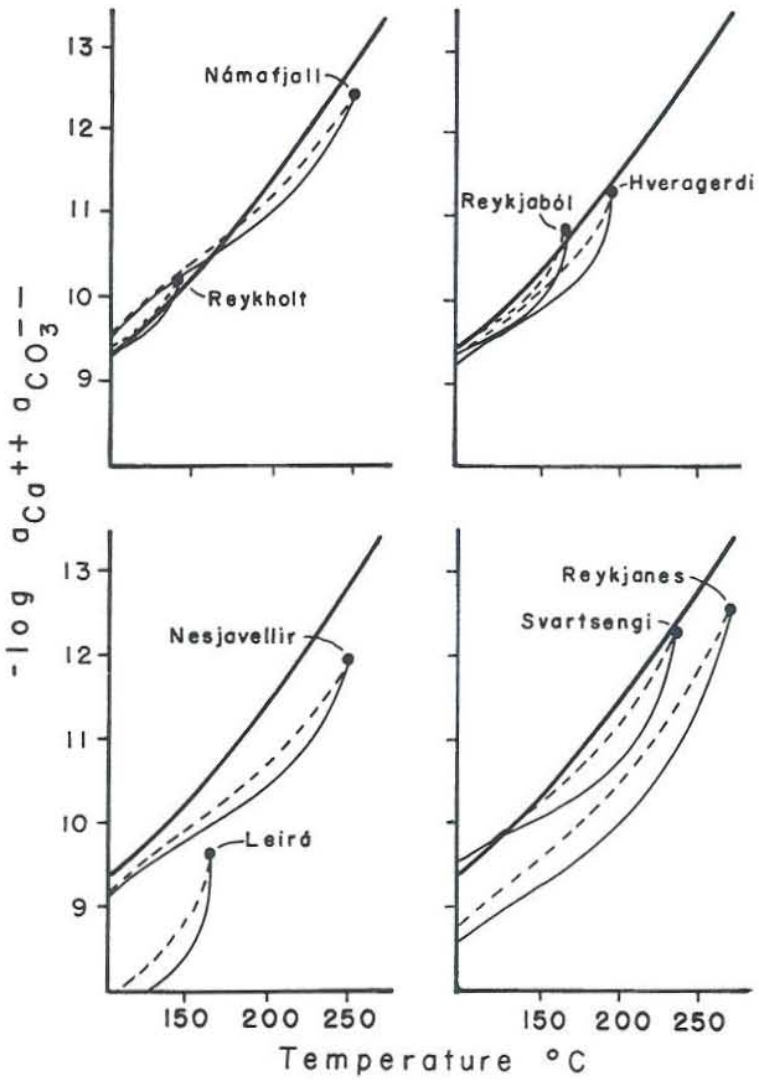

FIGURE 5. The computed activity product of Ca^{++} and $CO_3^{=}$ in geothermal waters during single-step adiabatic flashing in relation to the calcite solubility curve (thick solid line). The solid lines assume maximum degassing and the dashed lines 1/5 of maximum degassing. (From Arnorsson, 1978).

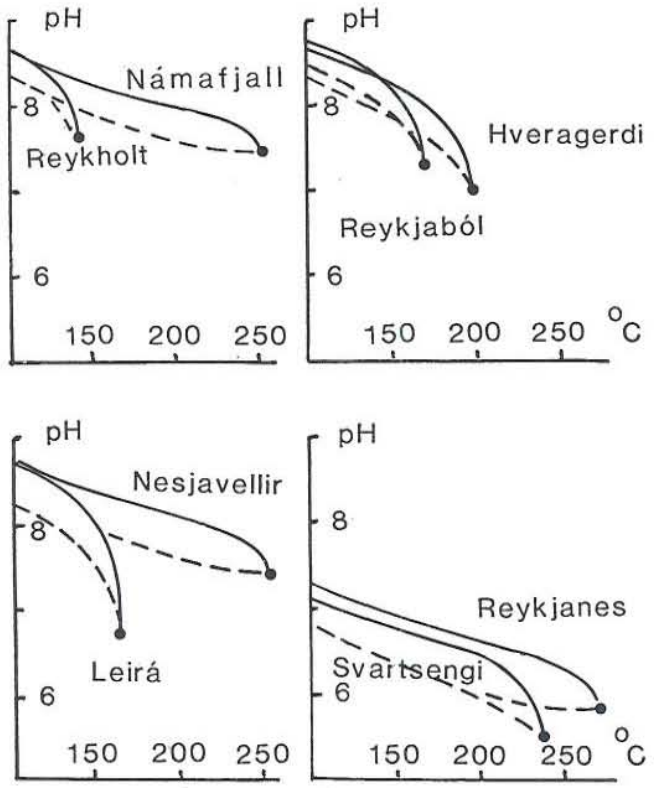

FIGURE 6. The variation in pH in geothermal waters during single-step adiabatic flashing in relation to the calcite solubility curve (thick solid line). The solid lines assume maximum degassing and the dashed lines 1/5 of maximum degassing. (Redrawn from Arnorsson, 1978).

SUMMARY

In most natural waters heating will cause calcite to precipitate, and cooling without boiling will cause it to dissolve (Fig. 4). However, where an ascending solution boils as a result of decompression (cooling adiabatically), carbonate is likely to precipitate as a result of the boiling (Fig. 5). The cooling that tends to move a solution toward a condition of undersaturation with respect to calcite is generally more than offset by the strong partitioning of CO_2 into the vapor phase (and concomitant decrease in partial pressure of CO_2) that decreases the solubility of calcite. At present, calculations that take account of all the physical processes (mainly boiling) and chemical reactions that influence the transport and deposition of carbonate minerals can be carried out only with the aid of sophisticated computer programs. However, if only the most abundant dissolved species in natural waters are considered, and simplifying assumptions are made about enthalpies of coexisting liquids and gases (mainly steam), hand-held, programmable calculators can be used effectively to calculate the approximate conditions for transport and deposition of calcite in hydrothermal solutions.

REFERENCES

Arnorsson, S., 1978, Precipitation of calcite from flashed geothermal waters in Iceland: Contrib. Mineral. Petrol., 66, 21-28.

Arnorsson, S., 1985, Gas pressure in geothermal systems: Chem. Geol., 49, 319-328.

Ellis, A.J., 1959, The solubility of calcite in carbon dioxide solutions: Am. J. Sci., 257, 354-365.

Ellis, A.J., 1963, The solubility of calcite in sodium chloride solutions at high temperatures: Am. J. Sci., 261, 259-267.

Ellis, A.J. and Golding, R.M., 1963, The solubility of carbon dioxide above 100°C in water and in sodium chloride solutions: Am. J. Sci., 261, 47-60.

Henley, R.W., Truesdell, A.H. and Barton, P.B., Jr., 1984, Fluid-mineral equilibria in hydrothermal systems: Rev. Econ. Geol., v. 1, 267 pp., Soc. Econ. Geol.

Keenan, J.H., Keyes, F.G., Hill, P.G. and Moore, J.G., 1969, Steam tables (international edition-metric units): New York, Wiley, 162 pp.

Svararsson, Hördur, 1981, The WATCH1 and WATCH3 programs -- Vehicles for interpreting chemical analyses of geothermal water. A guide for users. (Translated from Icelandic by Leo Kanner Assoc., 1983): Orkustofnun, Geothermal Division Report, 13 pp.

TABLE 1. Equations expressing the temperature dependence of various equilibrium constants and other coefficients that are described in the text. T is temperature in kelvins, and t is temperature in °C. The respective constants for equations (a) through (k) are given in Table 2. The data used in the derivation of these equations are shown in Table 3.

$$K_H = a + bT + cT^2 + dT^{-1} + e \log T \quad (a)$$

$$k = a + bT + cT^2 + dT^3 + e \log T \quad (b)$$

$$-\log K_1 = a + bT + cT^{-1} + d \log T \quad (c)$$

$$-\log K_2 = a + bT + cT^2 + dT^{-1} + e \log T \quad (d)$$

$$-\log K_0 = a + bT + cT^2 + dT^{-1} + e \log T \quad (e)$$

$$H_L = a + bt + ct^2 + dt^3 + et^4 + ft^5 + gt^{-1} + ht^{-2} + i \log t \quad (f)$$

$$H_G = a + bt + ct^2 + dt^3 + et^4 + ft^5 + gt^{-1} + ht^{-2} + i \log t \quad (g)$$

$$-\log K_c = a + bT + cT^2 + dT^3 + eT^{-1} \quad (h)$$

$$A = a + bT + cT^2 + dT^3 + eT^4 + fT^{-1} + g \log T \quad (i)$$

$$B = a + bT + cT^2 + dT^3 + eT^4 + fT^{-1} \quad (j)$$

$$-\log A_o = a + bT + cT^2 + dT^3 + eT^{-1} + fT^{-2} \quad (k)$$

$$\log PCO_{2(Total)} = 0.0053 - 621.4\ T^{-1} \quad (m)$$

TABLE 2. Coefficients for use with equations listed in Table 1.

K_H	-7646305	-3119.04939	1.091457	1.877554×10^{8}	3172908.8				
k	108.875	0.174114604	$-1.9845113 \times 10^{-4}$	1.0131668×10^{-7}	-58.867703				
$-\log K_1$	-124.4478	-0.0056623	5869.72601	45.589821					
$-\log K_2$	-143.4475	-0.0345539	1.9732326×10^{-5}	6161.87137	57.248899				
$-\log K_0$	130.5993	0.0517898	$-2.6766438 \times 10^{-5}$	-4417.6248	-51.47548				
H_L	414.44	10.2859	-0.05092	2.63085×10^{-4}	-6.93025×10^{-7}	7.4566×10^{-10}	-1209.757	11.98996	-353.764
H_G	2034.63	-5.04986	0.057399	-3.04263×10^{-4}	7.909545×10^{-7}	-8.69676×10^{-10}	1342.406	-13.2981	396.288
$-\log K_c$	-30.8131	0.1728295	-3.271501×10^{-4}	2.5529153×10^{-7}	2959.8903				
A	-11092.1143	-11.562984	0.01454757	$-1.2064489 \times 10^{-5}$	4.4598806×10^{-9}	176312.033	5229.515		
B	3.8096	-0.01846467	4.8075571×10^{-5}	$-6.0838461 \times 10^{-8}$	$3.0473184 \times 10^{-11}$	-126.7130669			
$-\log A_o$	1823.663	-3.9000818	0.004142503	-1.75503×10^{-6}	-421796.61	3.9002725×10^{7}			

TABLE 3. Values of dissociation constants, enthalpies of liquid water, H_L, and steam, H_G, and Debye-Hückel Coefficients, A and B, for the indicated temperatures. Enthalpy units are J/g. Units for A are $kg^{1/2}mole^{-1/2}$ and for B are $kg^{1/2}mole^{-1}cm^{-1}$.

t (°C)	100	125	150	175	200	225	250	275	300	Reference
K_H	5245	6150	6670	6860	6620		5340		3980	(1)
k	.078		.078		.089		.120		.178	(2)
$-\log K_1$	6.42	6.57	6.77	6.99	7.23	7.49	7.75	8.02	8.29	(1)
$-\log K_2$	10.16	10.25	10.39	10.57	10.78	11.02	11.29	11.58	11.89	(1)
$-\log K_0$	1.97		2.08		2.08		1.98		1.8*	(1)
H_L	419	525	632	741	852	967	1085	1210	1314	(3)
H_G	2676	2714	2746	2774	2793	2803	2802	2785	2749	(3)
$-\log K_c$	9.33		10.07		11.02		12.27		14.0*	(1)
A	.5998		.6898		.8099		.9785		1.2555	(1)
$B(x10^{-8})$	.3422		.3533		.3655		.3792		.3965	(1)
$-\log A_o$	3.71	3.41	3.13	2.86	2.58	2.31	2.05	1.78	1.51	(2)

* Extrapolated
(1) Henley et al. (1984)
(2) Ellis and Golding (1963)
(3) Keenan et al. (1969)

TABLE 4. Values of ionic charge, z, and ion-size parameter, $\overset{o}{a}$, for the common ionic species in geothermal fluids (from Henley et al., 1984).

	H^+	Na^+	HCO_3^-	HS^-	$H_3SiO_4^-$	$H_2BO_3^-$	F^-	$SO_4^=$	NH_4^+	HSO_4^-
z	1	1	1	1	1	1	1	1	1	1
$\overset{o}{a}(x10^8)$	9.0	4.0	4.5	4.0	4.0	4.0	3.5	4.0	2.5	4.0

	OH^-	$CO_3^=$	Cl^-	Li^+	K^+	Ca^{++}	Mg^{++}
z	1	2	1	1	1	2	2
$\overset{o}{a}(x10^8)$	4.0	4.5	3.5	6.0	3.0	6.0	8.0

THE SOLUBILITY OF SILICA IN HYDROTHERMAL SOLUTIONS: PRACTICAL APPLICATIONS

Robert O. Fournier
U.S. Geological Survey, Menlo Park, California 94025 U.S.A.

INTRODUCTION

The solubilities of the most common silica minerals have been determined experimentally as functions of temperature at the vapor pressure of the solution. Pressure and added salt have little effect on the solubilities of quartz and amorphous silica below about 300°C. Above 300°C, both pressure and added salt are very important. This information allows the dissolved silica concentration in a hydrothermal solution to be used as a chemical geothermometer. When using the silica geothermometer, an assumption must be made about the particular silica mineral that is controlling dissolved silica, and corrections may be required for the effects of decompressional boiling (adiabatic cooling). Also, below 340°C the solubility of silica decreases drastically as temperature decreases, so silica may precipitate from solution as a result of conductive or adiabatic cooling before reaching the surface, causing low estimated reservoir temperatures. In addition to causing problems in the application of the silica geothermometer, the precipitation of silica (scaling) can be a major problem during production and disposal of geothermal fluids. Therefore, the prediction of conditions at which silica polymerization and scaling will occur is of great importance in the design and operation of geothermal installations.

SILICA GEOTHERMOMETRY

The silica geothermometer of Fournier and Rowe (1966) was presented graphically as two curves that could be used in the range 120° to 330°C with the following assumptions: the fluid was in equilibrium with quartz in the reservoir, the pore-fluid pressure in the reservoir is fixed by the

vapor pressure of pure water (coexisting liquid and steam), there is no mixing of hotter and colder waters during upflow, and there is either conductive cooling of the ascending water or adiabatic cooling with steam separation at 100°C. Morey et al. (1962) noted that on a plot of log dissolved silica versus the reciprocal of absolute temperature, the data for quartz fall approximately along a straight line over the temperature range 20° to 250°C. Also, in the temperature range 20° to 250°C solubilities of chalcedony, α-cristobalite, β-cristobalite, and amorphous silica lie along nearly straight lines on a similar plot (Fig. 1). In addition, a plot of log dissolved silica (after steam separation at 100°C) versus the reciprocal of absolute temperature also is approximately a straight line in the range 90° to 250°C.

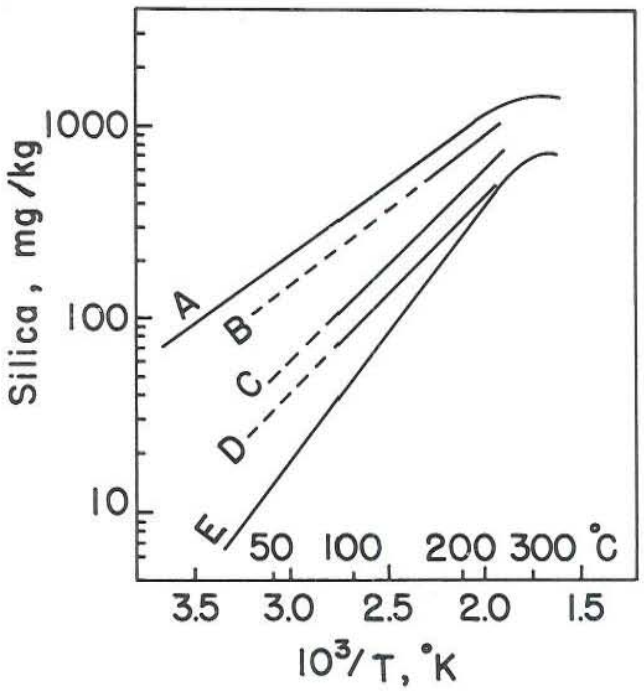

FIGURE 1. Solubilities of various silica phases in water at the vapor pressure of the solution. A = amorphous silica, B = opal-CT (incorrectly identified as β-cristobalite by Fournier, 1973), C = α-cristobalite, D = chalcedony, and E = quartz (from Fournier, 1973).

Chalcedony is a very fine-grained variety of quartz composed of aggregates of very tiny crystals. The individual quartz grains are so small that they have relatively large surface energies compared to "normal" quartz, and this results in an increase in solubility. Chalcedony is unstable in contact with water at temperatures above about 120-180°C because the smallest-sized crystals completely dissolve and larger-sized crystals grow large enough that surface energy is no longer a factor. Temperature, time, fluid composition, and prior history (recrystallization of amorphous silica versus direct precipitation of quartz), all affect the size attained by quartz crystals. Thus, in some places (particularly long-lived systems) well-crystalline quartz may control dissolved silica at temperatures less than 100°C, and in others chalcedony (very fine-grained quartz) may control dissolved silica at temperatures as high as 180°C (particularly younger systems).

Equations Applicable in the Temperature Range 20-250°C

Equations for the above straight lines (useful only for reservoir temperatures less than 250°C) are as follows, with the silica concentration, S, in mg/kg:

Quartz-no steam loss	$t°C = \frac{1309}{5.19 - \log S} - 273.15$	(1)
Quartz-maximum steam loss at 100°C	$t°C = \frac{1522}{5.75 - \log S} - 273.15$	(2)
Chalcedony	$t°C = \frac{1032}{4.69 - \log S} - 273.15$	(3)
α-Cristobalite	$t°C = \frac{1000}{4.78 - \log S} - 273.15$	(4)
β-Cristobalite	$t°C = \frac{781}{4.51 - \log S} - 273.15$	(5)
Amorphous silica	$t°C = \frac{731}{4.52 - \log S} - 273.15$	(6)

Figure 2 shows the solubility of quartz in water and coexisting steam at the vapor pressure of the solution up to the critical point of the very dilute solution. For comparison, the dotted line in Figure 2 shows the temperature-silica relations according to equation (1) above. Note the marked divergence of the calculated solubility using equation (1) from the actual solubility at temperatures above about 250°C.

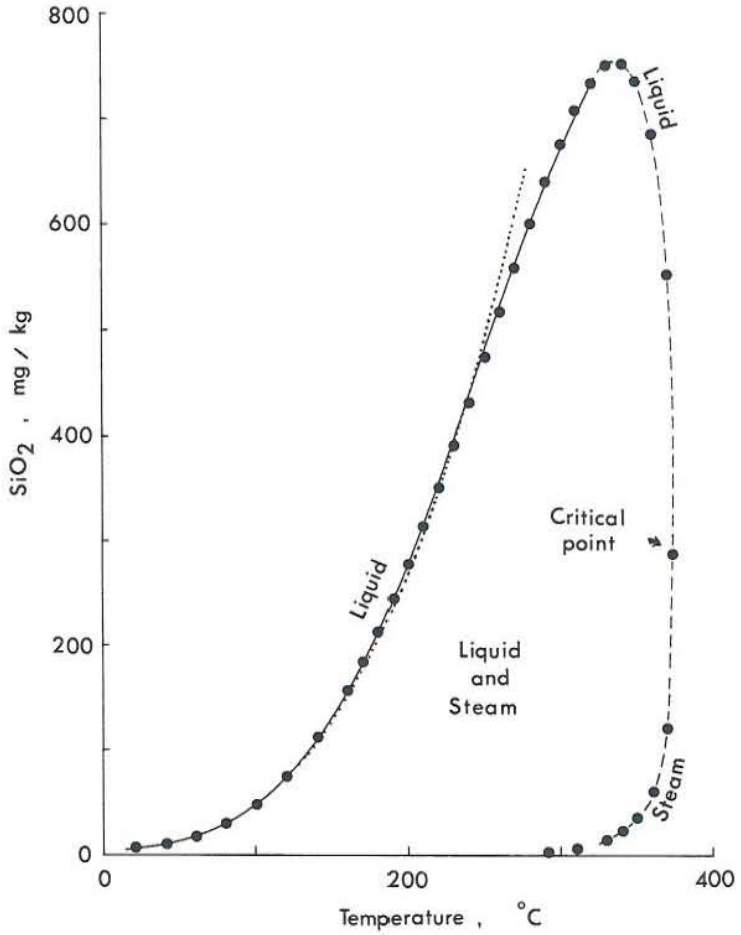

FIGURE 2. The solubility of quartz in water at the vapor pressure of the solution. The dots are points calculated using the equation of Fournier and Potter (1982a). The solid line is from equation (7), and the dashed line shows dissolved silica in liquid and steam outside the range of conditions for application of equation (7). The dotted line is from equation (1).

Quartz Geothermometer Equation Applicable in the Temperature Range 20-330°C

A silica (quartz) geothermometer equation given by Fournier and Potter (1982b) that is useful through the temperature range 20-330°C at the vapor pressure of the solution is

$$t°C = C_1 + C_2S + C_3S^2 + C_4S^3 + C_5 \log S \quad , \qquad (7)$$

where C_1 through C_5 are constants given in Table 1. Table 2 gives calculated quartz solubilities in liquid water and steam at the vapor pressure of the solution in 10°C temperature intervals up to the critical point. When there has been no steam separation, silica geothermometer temperatures can be obtained graphically from Figure 2 or computed from equation (7) up to 330°C. Note, however, that Figure 2 and equation (7) apply only to dilute solutions. High salinity of the solvent will have a minor effect on the solubility of quartz at temperatures below about 300°C and a major effect at higher temperatures (discussed later).

TABLE 1. Constants used in equations in the text.

	A_i Equation (9)	B_i Equation (10)	C_i Equation (7)	D_i Equation (8)
1.	4.1884×10^{2}	2.035×10^{3}	-4.2198×10^{1}	-3.5532×10^{0}
2.	1.0286×10^{1}	-5.0499×10^{0}	2.8831×10^{-1}	1.4600×10^{-1}
3.	-5.0920×10^{-2}	5.7399×10^{-2}	-3.6686×10^{-4}	-4.9270×10^{-4}
4.	2.6309×10^{-4}	-3.0426×10^{-4}	3.1665×10^{-7}	1.2305×10^{-6}
5.	-6.9303×10^{-7}	7.9095×10^{-7}	7.7034×10^{1}	-4.9421×10^{-10}
6.	7.4566×10^{-10}	-8.6968×10^{-10}		
7.	-1.2098×10^{3}	1.3424×10^{3}		
8.	1.1990×10^{1}	-1.3298×10^{1}		
9.	-3.5376×10^{2}	3.9629×10^{2}		

TABLE 2. Temperatures, enthalpies (Keenan et al., 1969), and silica solubilities (Fournier and Potter, 1982b) in liquid and gaseous water (steam) at the vapor pressure of the solution.

No.	T °C	H J/g	SiO_2 mg/kg	No.	T °C	H J/g	SiO_2 mg/kg	No.	T °C	H J/g	SiO_2 mg/kg
1.	20	84.0	6.1	18.	190	807.6	230.1	35.	360	1760.5	707.7
2.	30	125.8	8.1	19.	200	852.5	263.0	36.	370	1890.5	573.0
3.	40	167.6	10.7	20.	210	897.8	298.5	37.	374	2099.3	299.6
4.	50	209.3	14.0	21.	220	943.6	336.4	38.	370	2332.1	125.0
5.	60	251.1	18 2	22.	230	990.1	376.4	39.	360	2481.0	60.4
6.	70	293.0	23.5	23.	240	1037.3	418.3	40.	350	2536.9	35.4
7.	80	334.9	30.0	24.	250	1085.4	461.8	41.	340	2622.0	22.1
8.	90	376.9	37.9	25.	260	1134.4	506.2	42.	330	2665.9	14.1
9.	100	419.0	47.4	26.	270	1184.5	551.0	43.	320	2700.1	9.2
10.	110	461.3	58.6	27.	280	1236.0	595.3	44.	310	2727.3	6.0
11.	120	503.7	71.8	28.	290	1289.1	638.2	45.	300	2749.0	3.9
12.	130	546.3	87.1	29.	300	1344.0	678.4	46.	290	2766.2	2.5
13.	140	589.1	104.7	30.	310	1404.3	714.2	47.	280	2779.6	1.6
14.	150	632.2	124.6	31.	320	1461.5	743.6	48.	270	2789.7	1.0
15.	160	675.6	147.1	32.	330	1525.3	763.6	49.	260	2796.9	0.6
16.	170	719.2	172.1	33.	340	1594.2	770.1	50.	250	2801.5	0.4
17.	180	763.2	199.8	34.	350	1670.6	756.2	51.	240	2803.8	0.2

Possible Ambiguity at Very High Temperatures

The solubility of quartz at the vapor pressure of the solution reaches a maximum value of about 770 mg/kg at a temperature close to 338°C, and the solubility of quartz at the critical temperature is only about 300 mg/kg (Fig. 2). Therefore, for conductively cooled liquids, there are two possible initial reservoir temperatures when dissolved silica concentrations are above 300 mg/kg. One temperature is below 338°C and the other is above 338°C. However, from a practical point of view, silica geothermometry applied to hot-spring waters is not likely to give temperatures greater than 230° to 250°C because quartz dissolves and precipitates very quickly in response to changing temperature above about 230°C (Fournier, 1973; Rimstidt and Barnes, 1980). In the temperature range 250° to 330°C the silica geothermometer is most useful when applied to waters produced from geothermal wells where movement from the reservoir to the surface is rapid. Reservoir waters in natural hydrothermal systems having temperatures in excess of 330°C are very likely to be highly saline, so the curves and equations for dilute solutions would not be applicable.

DISSOLVED SILICA-ENTHALPY DIAGRAM

In contrast to temperature, enthalpy is a derived property that can be obtained from steam tables, provided that the temperature, pressure, and salinity are known. It is useful to use enthalpy as a coordinate rather than temperature because the combined heat contents (enthalpies) of two waters at different temperatures are conserved when those waters are mixed (neglecting small heat of dilution effects), but the combined temperatures are not. Figure 3 shows the solubility of quartz in pure water at the vapor pressure of the solution, plotted as a function of the enthalpy of the solution. In contrast to the silica-temperature plot (Fig. 2) in which there are two values for dissolved silica at a given temperature (in liquid and steam), in the silica-enthalpy plot there is only one value for dissolved silica at a given enthalpy. The solubility of quartz in steam is part of a bell-shaped, symetrical distribution of dissolved silica values that first increase to a maximum value at an enthalpy of about 1595 J/g, and then decrease with a further increase in enthalpy. For practical applications, most reservoir fluids are sufficiently dilute so that enthalpies of pure water can be used to construct enthalpy-composition diagrams.

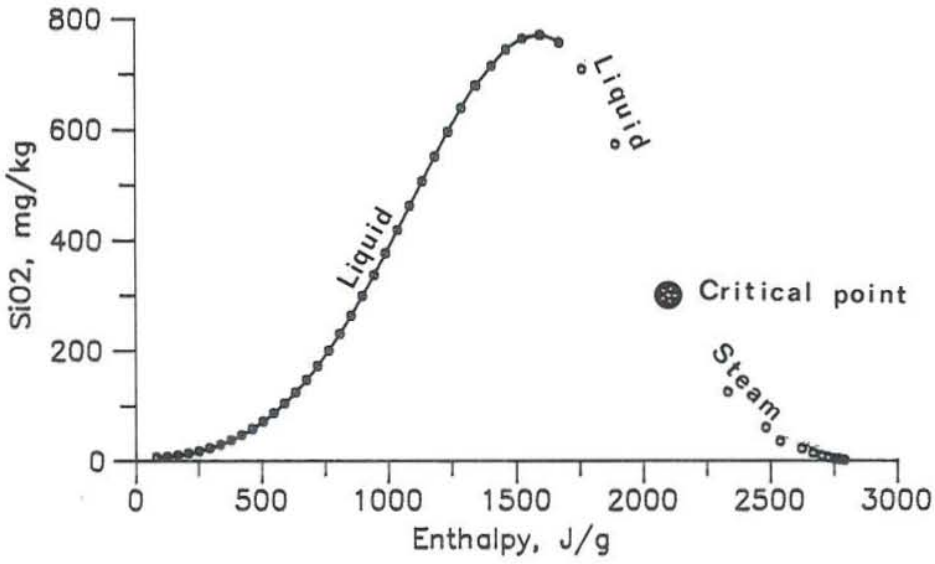

FIGURE 3. Solubility of quartz in water at the vapor pressure of the solution as a function of enthalpy.

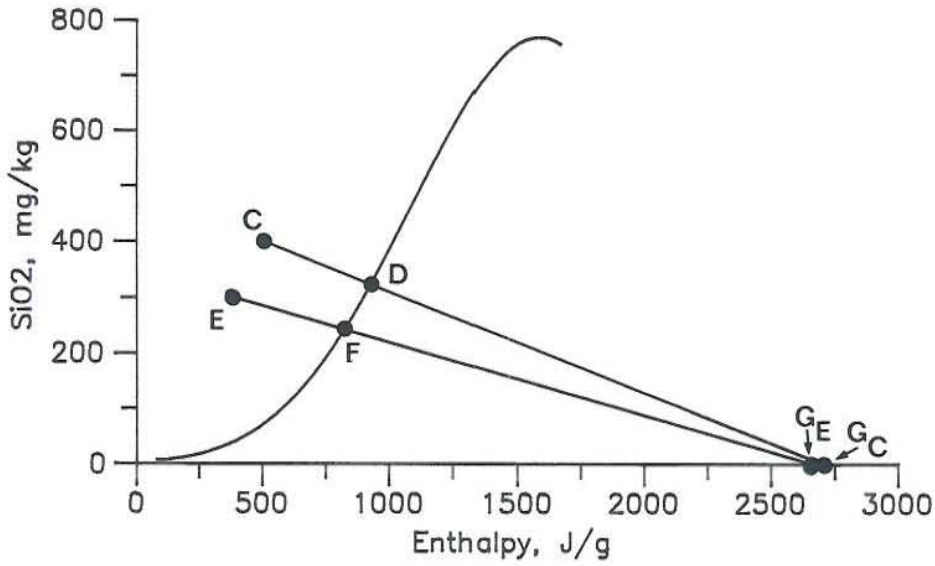

FIGURE 4. Enthalpy-silica graph illustrating use for calculating silica geothermometer temperatures of two waters that cooled adiabatically with single-stage steam loss at two different pressures. See text for discussion.

Silica Geothermometry with Adiabatic Cooling

Enthalpy-silica diagrams can be used to correct silica concentrations for adiabatic cooling with single-stage steam loss at any temperature. In Figure 4 line AB shows the solubility of quartz at the vapor pressure of the solution. Point E shows the silica concentration and enthalpy of the liquid water in a hypothetical vigorously boiling spring found at a high elevation where water boils at 90°C. Using steam tables, the enthalpy of liquid water at 90°C is found to be 376.9 J/g and that of the coexisting steam is 2660 J/g. Because steam contains less than 1 mg/kg dissolved silica at temperatures less than 265°C, point G_E characterizes the steam that separates from the boiling water of spring E. For a situation in which the water issuing from the spring cooled entirely by boiling (owing to decompression of the ascending fluid) and all the steam remained with the liquid until the steam-water mixture reached the surface (single-stage steam loss at 90°C), the silica concentration and enthalpy of the initial liquid water before boiling can be determined by finding the intersection of a straight line drawn between points E and G_E with the quartz solubility curve (point F in Fig. 4).

As a second example, consider a situation in which a wellhead steam-water separator operates at 1.99 bars (28.9 psia) vapor pressure of water (and, therefore, at a temperature of 120°C from steam tables). The separated liquid is then cooled quickly in an ice bath so that no additional vapor separates, and the silica concentration in the resulting water is found to be 400 mg/kg. The enthalpy of liquid water at 120°C is 503.7 J/g (point C in Fig. 4) and that of the coexisting steam is 2706 J/g (point G_C). The straight line drawn between C and G_C intersects the quartz solubility curve at point D, which characterizes the initial reservoir water.

Data for constructing the quartz solubility curve on an enthalpy-silica graph are given in Table 2. Alternately, an equation that expresses the solubility of quartz in liquid water at the vapor pressure of the solution as a function of the enthaply of the liquid water solvent is

$$S = D_1 + D_2H + D_3H^2 + D_4H^3 + D_5H^4, \qquad (8)$$

where S is silica concentration in mg/kg, H is enthalpy of liquid water in J/g, and D_1 through D_6 are constants given in Table 1. Equation (8) should not be used with enthalpies larger than 1670 J/g. Equations expressing the enthalpy of liquid water and steam at the vapor pressure of the solutions in the temperature range 50° to 340°C are

$$L = A_1 + A_2t + A_3t^2 + A_4t^3 + A_5t^4 + A_6t^5 + A_7t^{-1} + A_8t^{-2} + A_9\log t \qquad (9)$$

and

$$G = B_1 + B_2t + B_3t^2 + B_4t^3 + B_5t^4 + B_6t^5 + B_7t^{-1} + B_8t^{-2} + B_9\log t, \qquad (10)$$

where t is temperature in degrees Celsius, L and G are enthalpies of liquid water and steam, respectively, and A_1 through A_9 and B_1 through B_9 are constants given in Table 1. Do not use equations (9) and (10) to calculate enthalpies when $t < 50°C$. In the temperature range 0° to 50°C,

$$L = 4.1868\ t. \qquad (11)$$

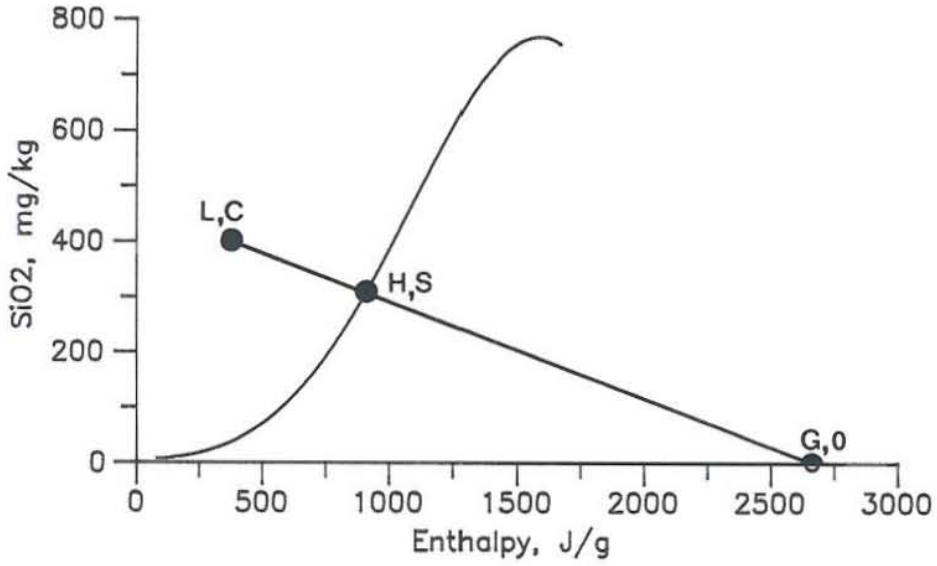

FIGURE 5. Enthalpy-silica relations showing general case for adiabatic cooling followed by steam loss at any temperature. See text for discussion.

Equations (7-10) allow a mathematical determination of silica geothermometer temperatures at any specified temperature with or without adiabatic cooling. Figure 5 shows a general case in which the coordinates of the initial reservoir water are (H,S), the coordinates of the liquid water after boiling and steam loss are (L,C), and the coordinates of the separated steam are (G,0). The equation for the straight line through these points is

$$S = - \frac{C}{(G - L)} (H - L) + C \ . \qquad (12)$$

Thus, there are two equations, (8) and (12), and two unknowns, S and H. These equations cannot be solved algebraically, but they can be solved easily with a computer using an iteration process.

THE SILICA MIXING MODEL

Under some circumstances the dissolved silica concentration of a mixed water and a silica-enthalpy diagram may be used to determine the temperature of the hot-water component (Fig. 6). A straight line drawn from a point representing the nonthermal component of the mixed water (point A, Fig. 6) through the mixed-water warm spring (point B) to the intersection with the quartz solubility curve gives the initial silica concentration and enthalpy of the hot-water component (point C). This procedure assumes that any steam that formed adiabatically (as the hot-water component moved up to a more shallow environment) did not separate from the residual liquid water before mixing with the cold-water component.

The following procedure can be used to determine the enthalpy and temperature of the hot-water component when steam was lost before mixing took place. For the situation in which steam was lost at atmospheric pressure prior to mixing (point D, Fig. 6), a horizontal line drawn from point D to the intersection with the maximum steam loss curve gives the initial enthalpy of the hot-water component (point E). The initial dissolved silica is shown by point F. If steam had been lost at a higher pressure before mixing, point D would lie above 419 J/g on the extension of line AB, and point E would lie between the maximum steam loss and quartz solubility curves.

In order for the above silica mixing model to give accurate results, it is vital that no conductive cooling occurred after mixing. If the mixed water cooled conductively after mixing, the calculated temperature of the hot-water component will be too high. It is also necessary that no silica deposition occurred before or after mixing and that quartz controlled the solubility of silica in the high-temperature water. Even with these restrictions the silica mixing model has been found to give good results in many places. In special circumstances, a silica mixing model could be used in which chalcedony or another silica phase is assumed to control the dissolved silica in the high-temperature component.

A mathematical solution may be obtained for the silica mixing model. In Figure 6, nonthermal ground water, point A, has a silica concentration A in a solution that has an enthalpy L_A. Similarly, the warm spring of "mixed" origin, point B, has a silica concentration B in a solution that

has an enthalpy L_B, and the reservoir fluid end member prior to mixing has a silica concentration C in a solution that has an enthalpy L_C. The equation for the straight line extending through points A and B to the intersection with the quartz solubility curve is

$$S = \frac{B - A}{L_B - L_A} (L_C - L_A) + A \ . \qquad (13)$$

Using equations (7), (8), (9), (11) and (13), the temperature of the hot-water component in the mixture can be calculated.

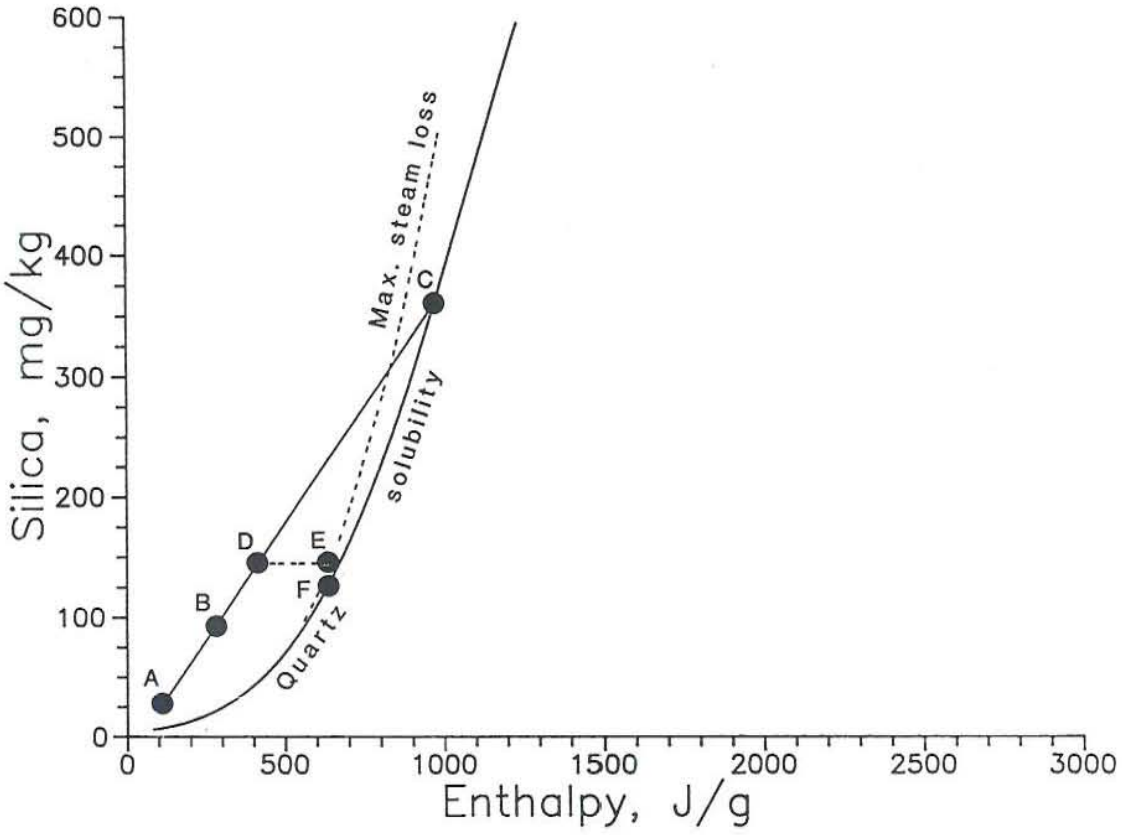

FIGURE 6. Enthalpy-silica graph illustrating use in calculating silica mixing model temperatures. See text for discussion.

GENERAL EQUATION FOR SOLUBILITY OF QUARTZ IN WATER, STEAM, AND SALINE SOLUTIONS APPLICABLE FROM 25° TO 900°C

The solubility of quartz in water in the temperature range 25° to 900°C at specific volume (V) of the solvent ranging from about 1 to 10 and from 300° to 600°C at specific volume of the solvent ranging from about 10 to 100 can be calculated using the following equations from Fournier and Potter (1982a), where $\underline{m}$ is molality dissolved silica and T is temperature in kelvins:

$$\text{Log } \underline{m} = A + B(\log V) + C(\log V)^2 \quad (14)$$

$$A = -4.66206 + 0.0034063\ T + 2179.7\ T^{-1} - 1.1292 \times 10^{6}\ T^{-2} + 1.3543 \times 10^{8}\ T^{-3} \quad (15)$$

$$B = -\ 0.0014180\ T - 806.9\ T^{-1} \quad (16)$$

$$C = 3.9465 \times 10^{-4}\ T \quad (17)$$

The solubility of quartz in natural saline solutions can be calculated using equation (14) when (- log ρF) is substituted for (log V), where ρ is the density of the solution and F is the weight fraction of water in that solution (Fournier, 1983). Note, however, that dissolved silica appears to form a complex with sulfate in sodium sulfate solutions, so additional calculations and adjustments are required when dealing with sulfate-rich brines (see Fournier and Marshall, 1983).

SOLUBILITY OF AMORPHOUS SILICA AT EXTREME CONDITIONS

Equation (6) can be rearranged to give the solubility of amorphous silica as a function of temperature for the range 0° to 250°C at the vapor pressure of the solution:

$$\text{Log } S = [-731/T] + 4.52\ , \quad (18)$$

where S is the concentration of dissolved silica in mg/kg and T is

temperature in kelvins. Molal solubilities ($\underline{m}$) of amorphous silica in the temperature range 90° to 340°C at the vapor pressure of the solution and at 1000 bars can be calculated using equations (19) and (20) (from Fournier and Marshall, 1983).

$$\text{V.P. solution} \quad \log \underline{m} = -6.116 + (0.01625\ T) - (1.758 \times 10^{-5}\ T^2) + (5.257 \times 10^{-9}\ T^3) \tag{19}$$

$$\text{1000 bars} \quad \log \underline{m} = -7.010 + (0.02285\ T) - (3.262 \times 10^{-5}\ T^2) + (1.730 \times 10^{-8}\ T^3) \tag{20}$$

The solubility of amorphous silica in saline solutions (m_s) at temperatures ranging from 100° to 340°C, and pressures ranging from the vapor pressure of the solution to about 1000 bars can be calculated using equations (21) and (22) where ρ_s is the density of the saline solution, $\rho°$ is the density of pure water at any given temperature and the indicated pressure (obtained from steam tables), and m° is the molal solubility in pure water obtained from equation (19) for the vapor pressure of the solution, and from equation (20) for 1000 bars (Fournier and Marshall, 1983).

$$\log m_s = -n \log \rho_s F + n \log \rho°_{(v.p.)} + \log m°_{(v.p.)} \tag{21}$$

$$n = \frac{[\log m°_{(1000\ bar)} - \log m°_{(v.p.)}]}{[\log \rho°_{(1000\ bar)} - \log \rho°_{(v.p.)}]} \tag{22}$$

EFFECTS OF pH

Decompressional boiling may result in loss of CO_2 and a corresponding increase in pH to values in excess of 8 or 9. High pH favors increased amounts of dissolved silica in solution. However, natural hydrothermal solutions generally have pH values of about 6 to 7 in the reservoir where water-rock equilibration has occurred at high temperatures. Therefore, in general a pH correction is not necessary for silica geothermometry. On the

other hand, an increase in pH accompanying adiabatic cooling may affect the silica scaling potential of a solution, so the effect of pH on the solubility of silica should be considered.

Dissolved silica hydrolyzes to form silicic acid, H_4SiO_4, and some of this silicic acid dissociates,

$$H_4SiO_4 = H_3SiO_4^- + H^+ . \tag{23}$$

The degree of dissociation of silicic acid as a function of pH can be determined as follows, where square brackets denote activities of the indicated species, K_1 is the first dissociation constant, $\underline{m}$ is molality, γ is the activity coefficient, and T is temperature in kelvins:

$$K_1 = \frac{[H_3SiO_4^-]\ [H^+]}{[H_4SiO_4]} , \tag{24}$$

$$K_1 = \frac{\underline{m}\ H_3SiO_4^- \times 10^{-pH}}{\underline{m}\ H_4SiO_4} \times \frac{\gamma\ H_3SiO_4^-}{\gamma\ H_4SiO_4} . \tag{25}$$

Values of $\gamma\ H_4SiO_4^-$ can be calculated using the Debye-Hückel equation. When $\underline{m}\ H_4SiO_4$ is determined using equation (14) and substituting $-\log \rho F$ for $\log V$, the value of $\gamma\ H_4SiO_4$ is unity.

Values of K_1 in the temperature range 0 to 350°C can be calculated using the following equation:

$$-\log K_1 = -631.8744 - .2967\ T + .000133266\ T^2 + 16705.03/T + 267.6478 \log T \tag{26}$$

For most natural thermal waters values of pH are too low for the second dissociation of silicic acid to be important, and

$$\underline{m}\ H_3SiO_4^- = \frac{\underline{m}\ SiO_2\ (total)}{\frac{10^{-pH}\gamma H_3SiO_4^-}{K_1} + 1} . \tag{27}$$

SILICA SCALING POTENTIAL AS A RESULT OF COOLING AND STEAM SEPARATION

Geothermal waters become supersaturated in respect to quartz when they cool with or without boiling as they flow from a region of higher temperature and pressure (the reservoir) to a region of lower temperature and pressure (generally the earth's surface or a steam separator that operates at a given pressure). During the exploitation of geothermal resources silica scaling generally occurs only when and where a cooling hydrothermal solution becomes supersaturated in respect to amorphous silica. This may occur within piping and other equipment at the surface or within the well. The specific conditions at which silica scale is likely to form as a result of conductive or adiabatic cooling of a given reservoir fluid can be shown nicely with the aid of a silica-enthalpy diagram (Fig. 7). Figure 7 shows the solubility of quartz at pH 7 or less (should apply to most reservoir fluids) and the solubility of amorphous silica at selected values of pH as functions of enthalpy.

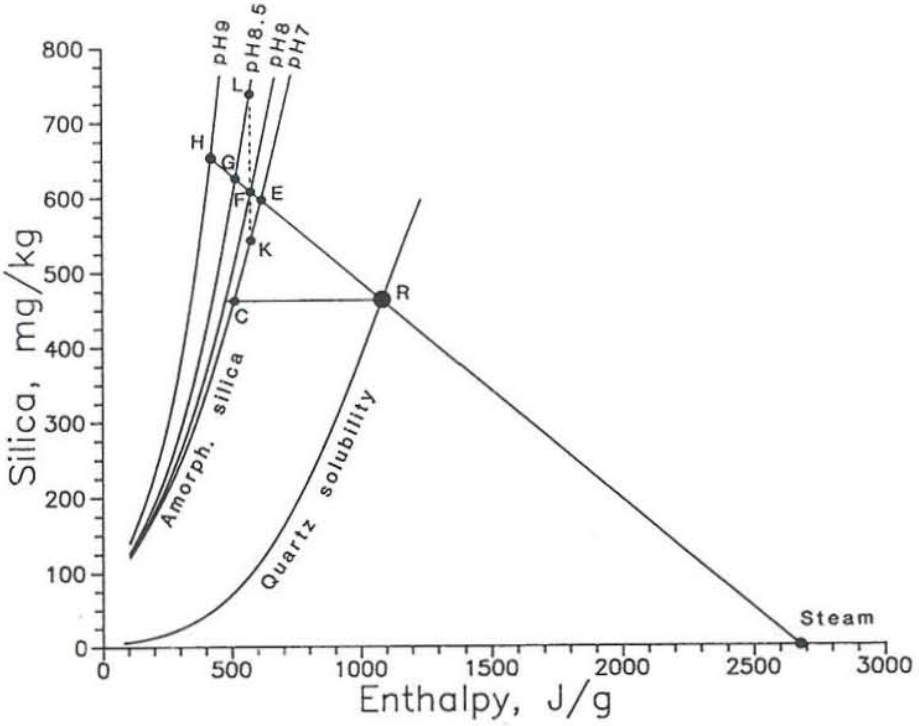

FIGURE 7. Dissolved silica-enthalpy diagram showing solubility of quartz at pH 7 and solubility of amorphous silica at various indicated values of pH. See text for discussion.

Consider a relatively dilute fluid in equilibriun with quartz in a reservoir at a temperature of 250°C (point R in Fig. 7). At that temperature and at the vapor pressure of the solution, liquid has an enthalpy of about 1085 J/g and contains about 462 mg/kg dissolved silica. Conductive cooling during upflow (perhaps to a hot spring that has a relatively slow rate of discharge) without precipitation of a crystalline silica phase, such as quartz or cristobalite, will result in the solution becoming just saturated in respect to amorphous silica when the enthalpy decreases to about 520 J/g at a pH of 7 or less (point C in Fig. 7 at a temperature of about 124°C). Further cooling with no increase in pH will result in the solution becoming supersaturated in respect to amorphous silica, and that phase may precipitate. However, the initial partial pressure of CO_2 in the reservoir fluid at 250°C is about 2.35 bars (obtained from an equation given by Arnorsson, 1985), so there could be a slight increase in pH during conductive cooling if CO_2 is lost because of fluid decompression. For a situation in which a solution cools conductively from 250°C with an accompanying increase in pH to 8 because of loss of CO_2, that solution would become just saturated in respect to amorphous silica at an enthalpy of about 480 J/g (about 115°C), which is 60 J/g and 9°C lower than for the situation in which there is no increase in pH.

For commercial situations, cooling of the ascending fluid is likely to be mainly by decompressional boiling (adiabatic) and the pH is likely to increase during upflow because of CO_2 partitioning into the steam phase. For adeabatic cooling of reservoir fluid R in Figure 7, the boiling solution becomes just saturated in respect to amorphous silica at an enthalpy of about 620 J/g at pH 7 (point E with a temperature of 147°C), 575 J/g at pH 8 (point F with a temperature of 137°C), 520 J/g at pH 8.5 (point G with a temperature of 124°C), and 425 J/g at pH 9 (point H with a temperature of 102°C). Assume that a wellhead steam separator is designed to operate at a pressure of 3.3 bars (residual liquid enthalpy equal to 575 J/G after steam separation). If the pH of the flashed fluid does not exceed 7, the residual liquid in the separator (point F) would be supersaturated in respect to the solubility of amorphous silica (point K) by about 70 mg/kg and silica scaling would likely result. On the other hand, if the solution pH increased to 8 as a result of CO_2 separation into the steam phase, the solution would be just saturated in respect to amorphous silica at point F

and no silica scaling will occur in the separator as long as the pressure is maintained at or higher than 3.3 bars. Note that if the solution pH increases to as high as 8.5 as a result of CO_2 partitioning into the steam phase, the solution at point F would be about 125 mg/kg below saturation in respect to the solubility of amorphous silica (point L), and steam separation could be carried out at a pressure as low as 2.25 bars (point G) without silica scaling.

CONCLUSIONS

Equations are presented here that allow calculation of the solubility of quartz at any temperature and pressure of geologic interest, and in any saline solution (except Na_2SO_4-rich solutions that complex dissolved silica), provided the solution density is known at the temperature and pressure of interest. It is recommended that equation (7) be used for silica (quartz) geothermometry. Equation (3) should be used for silica (chalcedony) geothermometry, and equation (19) should be used to calculate the solubility of amorphous silica at the vapor pressure of the solution. Enthalpy-silica diagrams (or computer programs based on enthalpy-silica relations) should be used to take account of the effects of boiling and mixing of different waters, and to calculate scaling potentials. In calculating silica scaling potentials, account must be taken of the possible increases in pH resulting from partitioning of CO_2 into the steam phase.

REFERENCES

Arnorsson, S., 1985, Gas pressure in geothermal systems: Chem. Geol., 49, p. 319-328.

Fournier, R. O., 1973, Silica in thermal waters: Laboratory and field investigations, in Proceedings, International Symposium on Hydrogeochemistry and Biogeochemistry, Tokyo, 1970, v. 1, Hydrogeochemistry: Washington, D.C., Clark, pp. 122-139.

Fournier, R.O., 1977, Chemical geothermometers and mixing models for geothermal systems: Geothermics, 5, 41-50.

Fournier, R.O., 1983, A method of calculating quartz solubilities in aqueous sodium chloride solutions: Geochim. Cosmochim. Acta., 47, 579-586.

Fournier, R. O. and Marshall, W. L., 1983, Calculation of amorphous silica solubilities at 25° to 300°C and apparent cation hydration numbers in aqueous salt solutions using the concept of effective density of water: Geochim. Cosmochim. Acta, 47, 587-596.

Fournier, R.O. and Potter, R.W., II, 1982a, An equation correlating the solubility of quartz in water from 25° to 900°C at pressures up to 10,000 bars: Geochim. Cosmochim. Acta., 46, 1969-1974.

Fournier, R. O. and Potter, R. W., II, 1982b, A revised and expanded silica (quartz) geothermometer: Geotherm. Resourc. Counc. Bull., 11(10), 3-12.

Fournier, R.O. and Rowe, J.J., 1966, Estimation of underground temperatures from the silica content of water from hot springs and wet-steam wells: Am. J. Sci., 264, 685-697.

Morey, G.W., Fournier, R.O. and Rowe, J.J., 1962, The solubility of quartz in water in the temperature interval from 25° to 300°C: Geochim. Cosmochim. Acta, 26, 1029-1043.

Rimstidt, J.D., and Barnes, H.L., 1980, The kinetics of silica-water reaction: Geochim. Cosmochim. Acta, 44, 1683-1699.

CATION GEOTHERMOMETRY

Robert O. Fournier
U.S. Geological Survey, Menlo Park, California 94025 U.S.A.

INTRODUCTION

Cation geothermometers are widely used to interpret compositions of waters collected from hot springs and wells. At this time there are many different geothermometers to choose from and it is rare when they all give about the same result, especially when applied to hot-spring waters. This presentation will discuss the bases for cation geothermometers and general precautions in their application. Equations for the various geothermometers that are now in use are given in Table 1.

THE THEORETICAL BASIS FOR CATION GEOTHERMOMETRY

Cation geothermometry is based on ion exchange reactions that have temperature-dependent equilibrium constants. An example is exchange of Na^+ and K^+ between coexisting alkali feldspars:

$$NaAlSi_3O_8 + K^+ = KAlSi_3O_8 + Na^+ . \qquad (1)$$

The equilibrium constant, K_{eq}, for reaction (1) is

$$K_{eq} = \frac{[KAlSi_3O_8][Na^+]}{[NaAlSi_3O_8][K^+]} , \qquad (2)$$

where square brackets denote activities of the enclosed species. In the application of equation (2), usual simplifying assumptions are that the activities of the solid reactions (in this case albite and K-feldspar) are unity and that activities of the dissolved species are about equal to their molal concentrations in aqueous solution (generally a good assumption only

TABLE 1. Equations for cation geothermometers (concentrations in mg/kg).

Geothermometer	Equation		Source
Na-K	$t°C = \frac{856}{0.857 + \log(Na/K)} - 273.15$		Truesdell (1976)
Na-K	$t°C = \frac{883}{0.780 + \log(Na/K)} - 273.15$		Tonani (1980)
Na-K	$t°C = \frac{933}{0.993 + \log(Na/K)} - 273.15$	(25-250°C)	Arnorsson (1983)
Na-K	$t°C = \frac{1319}{1.699 + \log(Na/K)} - 273.15$	(250-350°C	Arnorsson (1983)
Na-K	$t°C = \frac{1217}{1.483 + \log(Na/K)} - 273.15$		Fournier (1983)
Na-K	$t°C = \frac{1178}{1.470 + \log(Na/K)} - 273.15$		Nieva (1987)
Na-K	$t°C = \frac{1390}{1.750 + \log(Na/K)} - 273.15$		Giggenbach (1988)
K-Mg	$t°C = \frac{4410}{14.00 + \log(K/\sqrt{Mg})} - 273.15$		Giggenbach (1988)
K-Li	$t°C = \frac{2200}{5.470 - \log(Li/\sqrt{Mg})} - 273.15$		Kharaka & Mariner (1988)
Na-Li	$t°C = \frac{1590}{0.779 + \log(Na/Li)} - 273.15$		Kharaka et al. (1982)
Na-Li (Cl<0.3M)	$t°C = \frac{1000}{0.389 + \log(Na/Li)} - 273.15$		Fouillac & Michard (1982)
Na-Li (Cl>0.3M)	$t°C = \frac{1195}{0.130 + \log(Na/Li)} - 273.15$		Fouillac & Michard (1982)
Na-Ca	$t°C = \frac{1096.7}{2.370 - \log(Na/\sqrt{Ca})} - 273.15$		Tonani (1980)
K-Ca	$t°C = \frac{1930}{2.920 - \log(K/\sqrt{Ca})} - 273.15$		Tonani (1980)
Na-K-Ca	$t°C = \frac{1647}{\log(Na/K)+\beta[\log(\sqrt{Ca}/Na)+2.06]+2.47} - 273.15$		Fournier & Truesdell (1973)

$\beta = 4/3$ for $t<100°C$; $= 1/3$ for $> 100°C$

for dilute solutions). Thus, equation (2) reduces to

$$K_{eq} = Na/K \ , \tag{3}$$

where Na and K are molalities of the respective ions. Concentrations of the dissolved constituents also can be expressed in other units, such as milliequivalents, ppm, or mg/kg, with the value of K_{eq} adjusted accordingly. For an exchange reaction involving monovalent and divalent ions, such as two K^{+} and one Mg^{+2}, the equilibrium constant is approximately equal to

$$K_{eq} = K/\sqrt{Mg} \ . \tag{4}$$

The variation of the equilibrium constant with temperature is given by an integrated form of the van't Hoff equation,

$$\log K_{eq} = \frac{\Delta H^{\circ}}{2.303RT} + C \ , \tag{5}$$

where ΔH° is the differential heat of solution, T is temperature in kelvins, R is the gas constant, and C is a constant of integration. The value of ΔH° generally changes little with temperature in the range 0-300°C, so a plot of log K_{eq} (equal to log Na/K for reaction 1 above) versus 1000/T gives an approximately straight line.

Let us return to the assumption that activity coefficients of the solid reactants are unity (required to reduce equation 2 to equation 3). This assumption is true when the reactants have pure end-member compositions. In natural systems, however, many different cations commonly exist in solid solution within certain types of silicates, such as Na and Ca in plagioclase and Na, Ca, Mg, K, and Li in montmorillonites. By writing reactions in terms of the pure end-member components we tend to ignore the existence and consequences of solid solutions. When a solid solution, such as plagioclase, reacts with K^{+} to form K-feldspar plus a more calcic silicate plus Na^{+}, the activity coefficient of the Na-component of the Na-Ca silicate is not unity. Not taking into account effects of solid solutions contributes to inconsistencies in cation geothermometry, and the Na/K geothermometer in particular.

NA/K GEOTHERMOMETERS

The Na/K geothermometer is generally thought to take longer to reach equilibrium at a given temperature than other commonly used geothermometers. Therefore, the Na/K ratio is commonly used to estimate possible highest temperatures in deeper parts of a system where waters reside for relatively long periods of time, and other geothermometers are used to estimate lower temperatures that occur in shallower reservoirs where waters reside for relatively short periods of time. This may be an appropriate use of the geothermometer when applied to some well waters, but is a dangerous practice when applied to hot-spring waters.

Figure 1 shows log (Na/K) versus 1000/T for base exchange between albite and adularia, and between albite and microcline, calculated using equilibrium constant equations published by Arnorsson (1982). Positions of empirical Na/K geothermometers suggested by various authors also are shown in Figure 1. Three of these geothermometers (Truesdell, 1976; Tonani, 1980; Arnorsson, 1983) give essentially the same result while the Na/K geothermometers of Nieva (1987), Fournier (1979) and Giggenbach (1988) give significantly higher temperatures for reservoir waters below about 300°C. Note that all of these empirical Na/K geothermometers lie between the albite-microcline and albite-adularia curves. The data points that were used in the determination of these empirical geothermometers (different data sets for the different geothermometers) also lie in a broad band between the albite-microcline and albite-adularia curves, and show the greatest amount of scatter at lower temperatures. All of the empirical geothermometers give about the same result at about 300°C.

A considerable range in structural states of alkali feldspars may persist metastably at low temperatures, and base exchange involving different kinds of K-feldspar can explain the entire range of Na/K values exhibited by the data and the various empirical Na/K geothermometers. Also, other minerals may participate in cation exchange reactions involving Na and K, such as Na- and K-montmorillonites,

$$Na_{.33}Al_2(Al_{.33}Si_{3.67}O_{10})(OH)_2 + .33K^+ = K_{.33}Al_2(Al_{.33}Si_{3.67}O_{10})(OH)_2 + .33Na^+ , \qquad (6)$$

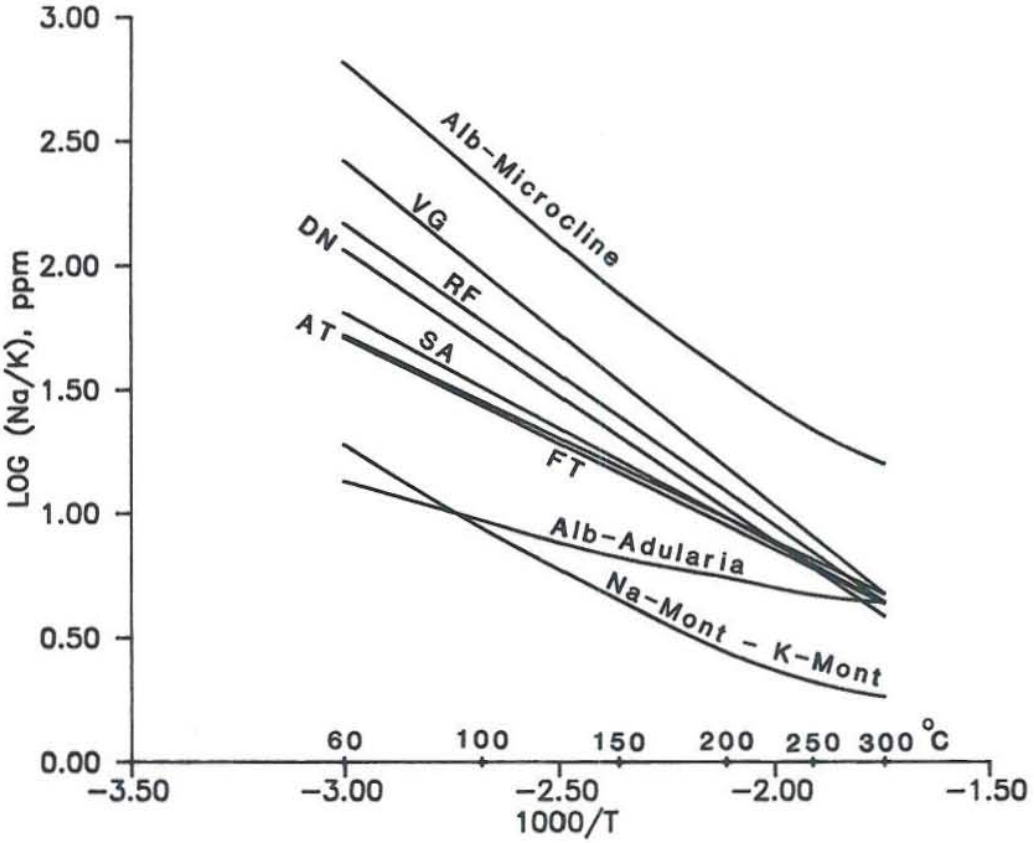

FIGURE 1. Variation of log (Na/K) as a function of the reciprocal of absolute temperature. Theoretical curves for low albite - microcline, low albite - adularia, and Na-montmorillonite - K-montmorillonite calculated using equilibrium constants in Arnorsson (1982). Various Na/K geothermometers are labeled VG (Giggenbach, 1988), RF (Fournier, 1979), SA (Arnorsson, 1983), AT (Truesdell, 1976), FT (Tonani, 1980).

and the equilibrium constant for reaction (6) also is equal to the activity ratio Na/K. However, the Na/K ratio that results from exchange involving just montmorillonites at a given temperature is generally different from that involving just alkali feldspars (see Fig. 1). In addition, it is likely that in some places (particularly low-temperature environments) albite may not be present and a reaction involving K-feldspar, sodic clay, and H^+ may control Na/K, such as

$$3\ \text{Na-Montmorillonite} + 7K^+ + 10\ \text{Quartz} = 7\ \text{K-spar} + \text{Na} + 6H^+ \ . \qquad (7)$$

When the activity coefficients of the solid reactants are unity, the equilibrium constant for reaction (7) is

$$K_{eq} = \frac{[Na^+][H^+]^6}{[K^+]^7} \qquad (8)$$

and

$$\text{Log } K_{eq} = \text{Log } [Na/K] - 6 \text{ Log } [K/H] \; . \qquad (9)$$

From the above discussion, we may conclude that there is no single universally best Na/K geothermometer because one may give the correct temperature in one place and an erroneous temperature in another, depending on the particular mineral assemblage (and structrual states of the minerals) with which the circulating water equilibrates. Also, as a further note of caution, the Na/K geothermometer tends to give anomalously high temperatures when applied to NH_4-rich waters that have reacted with organic-rich sediments.

THE NA-K-CA GEOTHERMOMETER

The Na-K-Ca geothermometer (Fournier and Truesdell, 1973) takes account of reactions involving exchange of Na^+, K^+, and Ca^{+2} with mineral solid solutions. This minimizes effects of disregarding activity coefficients of solids. The geothermometer is entirely empirical and assumes one type of base exchange reaction at temperatures above about 100°C,

$$K^+ + Na_{2/3}Ca_{1/6}\text{-solid} = (1/6)Ca^{+2} + (2/3)Na^+ + K\text{-solid} \; , \qquad (10)$$

and a different exchange reaction at temperatures below about 100°C,

$$K^+ + (1/3)Na^+ + Ca_{2/3}\text{-solid} = (2/3)Ca^{+2} + KNa_{1/3}\text{-solid} \; . \qquad (11)$$

The general form of both of the above reactions is

$$\log K_{eq} = \log (Na/K) + \beta \log (Ca^{1/2}/Na) \; , \qquad (12)$$

where β is 1/3 for waters equilibrating above about 100°C and 4/3 for waters equilibrating below about 100°C. An exception to the above rule is that β equals 1/3 should be used for waters less than 100°C when log ($Ca^{1/2}/Na$) is negative, with concentrations of dissolved constituents expressed in molality units.

It is likely that base exchange involving clays and micas is a major controlling factor in fixing Na-K-Ca concentrations in natural waters. The Na-K-Ca geothermometer appears to give excellent results for most waters above about 200°C, but erratic results are obtained for lower-temperature waters. These erratic results appear to come from effects of high partial pressures of CO_2 and exchange reactions involving Na^+, K^+, or Ca^+ with additional ions (particularly Mg). Another likely source of error is precipitation of calcium as carbonate where solutions boil on the way from the reservoir to the surface. Precipitation of Ca generally will result in estimated temperatures that are too high.

Effect of Carbon Dioxide

Various authors have concluded that the Na-K-Ca geothermometer is sensitive to the partial pressure of CO_2 (see Giggenbach, 1988 for a review). For aquifer temperatures less than 75°C and partial pressures of $CO_2 > 10^{-4}$ Paces (1975) recommended that the Na-K-Ca geothermometer be modified to include an extra parameter, $\underline{I}$,

$$\log K_{eq} = \log (Na/K) + (4/3)\log (Ca^{1/2}/Na) + \underline{I} , \qquad (13)$$

$$\underline{I} = -1.36 - 0.253 \log P_{CO_2} . \qquad (14)$$

Apparently the Na-K-Ca geothermometer generally works well at temperatures above about 200°C because in most geothermal reservoirs the partial pressure of CO_2 varies systematically with temperature. Below 200°C the Na-K-Ca geothermometer should be applied with caution to CO_2-rich waters. Dilute, $NaHCO_3$-rich waters may be particularly troublesome because plagioclase may be completely converted to clay (including kaolinite) at a relatively high pH (5-6) with the resulting water compositions considerably off the empirical temperature-fluid composition trends that have been established for Cl-rich geothermal fluids.

The Mg Correction for the Na-K-Ca Geothermometer

Fournier and Potter (1979) noted that when the Na-K-Ca geothermometer is applied to Mg-rich waters it commonly gives temperatures that are too high. In an attempt to overcome this problem they devised a Mg correction based on a variable R that is defined in Table 2. Equations for calculating the Mg correction for values of R between 0.5 and 5 and 5 and 50 are given in Table 2.

TABLE 2. Equations for calculating the Mg correction for the Na-K-Ca geothermometer. Concentrations, C, are in mg/kg.

$$R = \frac{C_{Mg}}{C_{Mg} + 0.61C_{Ca} + 0.31C_{K}} \times 100$$

For R from 1.5 to 5,

$$\Delta t_{Mg}\,°C = 1.03 + 59.971\log R + 145.05(\log R)^2 - 36711(\log R)^2/T - 1.67 \times 10^7 \log R/T^2$$

For R from 5 to 50,

$$\Delta t_{Mg}\,°C = 10.66 - 4.7415\log R + 325.87(\log R)^2 - 1.032 \times 10^5(\log R)^2/T - 1.968 \times 10^7(\log R)^2/T^2 + 1.605 \times 10^7(\log R)^3/T^2$$

Note - Do not apply a Mg correction if Δt_{Mg} is negative or <1.5.

Mg concentrations in geothermal fluids decrease rapidly as temperature increases and all Mg-rich fluids found in nature have undergone water-rock reaction at a relatively low temperature. Furthermore, as geothermal fluid flows from a high-temperature environment to lower temperatures, it appears to pick up significant amounts of Mg from the surrounding rock relatively easily and quickly. This leads to major ambiguity in the application of the Fournier and Potter (1979) Mg correction; that is, a truly low-temperature water may require a Mg correction to give a correct temperature, but a Mg correction applied to a high-temperature water that has picked up Mg during upflow will yield too low a reservoir temperature. The best way to deal with these ambiguities is to sample and analyze many different springs and wells, and to use a combination of silica and various cation geothermometers to evaluate possible mixing of different waters and possible retrograde reactions that may occur during upflow.

K/√MG AND LI/√MG GEOTHERMOMETERS

Exchange reactions involving Mg appear to proceed relatively fast at low temperatures and K/√Mg and Li/√Mg ratios appear to be good indicators of the last temperature of water-rock equilibration. When there is good agreement in the temperatures estimated using K/√Mg (Giggenbach, 1988), Li/√Mg (Kharaka and Mariner, 1988), and other geothermometers (particularly Na-K-Ca and silica), one can be fairly certain that water-rock equilibration has occurred at that temperature and that there has been little water-rock reaction during subsequent flow to the surface. Agreement between K/√Mg and Li/√Mg geothermometer temperatures, but higher temperatures estimated using other geothermometers, may indicate a relatively short time in reservoir at intermediate depth and intermediate temperature where water-rock reequilibration occurs only in respect to the most reactive phases. Disagreement among all the geothermometers may result from mixing of different waters without water-rock reequilibration after mixing.

OTHER CATION GEOTHERMOMETERS

Various other cation geothermometers have been proposed that may be of use in some situations. These include Na/√Ca (Tonani, 1980), K/√Ca (Tonani, 1980), and Na/Li (Fouillac and Michard, 1981; Kharaka et al., 1982). The problem of applying cation ratios involving Ca to estimate temperatures of CO_2-rich waters has been previously discussed. It is likely that Na/√Ca and K/√Ca will be affected by variations in CO_2 partial pressure to an even greater extent than is the Na-K-Ca geothermometer, and Giggenbach (1988) uses K/√Ca mainly as an indicator of CO_2 partial pressure. Note, that precipitation of calcium carbonate from an ascending fluid will cause the Na/√Ca and K/√Ca geothermometer temperatures to be too high and also will cause the estimated CO_2 partial pressure to be too high.

The Na/Li geothermometers proposed by Fouillac and Michard (1981) and Kharaka et al. (1982) commonly give very different results when applied to the same water. Furthermore, this geothermometer appears to be particularly sensitive to total dissolved solids and to rock type. Because Li is generally a relatively minor constituent in a geothermal fluid and Na is generally a major constituent, slight changes in Li that result from exchange involving ions other than Na can greatly affect the Na/Li ratio. Thus, the Na/Li ratios may be accidental, a secondary result of these other reactions.

NA-K-MG-CA GEOINDICATORS

Giggenbach (1988) suggested that a triangular diagram with Na/1000, K/100, and √Mg at the apices can be used to classify waters as fully equilibrated with rock at given temperatures, partially equilibrated, and immature (dissolution of rock with little or no chemical equilibrium), as shown in Figure 2. In addition he uses a plot of log (K^2/Ca) versus log (K^2/Mg) to estimate CO_2 fugacities or partial pressures (Fig. 3). Figure 2 may be a better way to assess effects of Mg on fluid compositions than the cumbersome Mg correction to the Na-K-Ca geothermometer proposed by Fournier and Potter (1979).

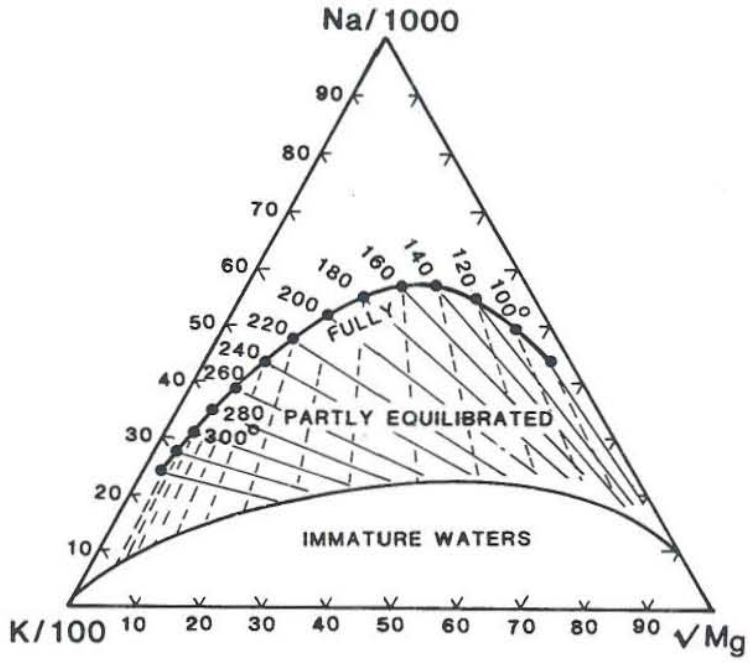

FIGURE 2. Diagram for evaluating Na/K and K/√Mg temperatures in geothermal waters (from Giggenbach, 1988). See text for discussion.

The general approach presented by Giggenbach (1988) is recommended, but with some words of caution. In Figure 2 the temperatures and compositions at which "full equilibration" is shown may change significantly, depending on which of the many Na/K geothermometers one assumes are correct and the mineralogy (including structural states) of the phases that are in contact with the reservoir fluid. For relatively acid conditions in which albite has been completely altered to mica and clay, the temperatures that one derives using Figure 2 may be considerably in error. The main significance of Figure 2 is that it can be used to draw attention to waters that are only in partial equilibrium with rock, either as a result of mixing or water-rock reactions during upflow. Figure 2 also can be used to distinguish immature waters that should not be used for cation geothermometry from waters that can provide information about subsurface thermal conditions.

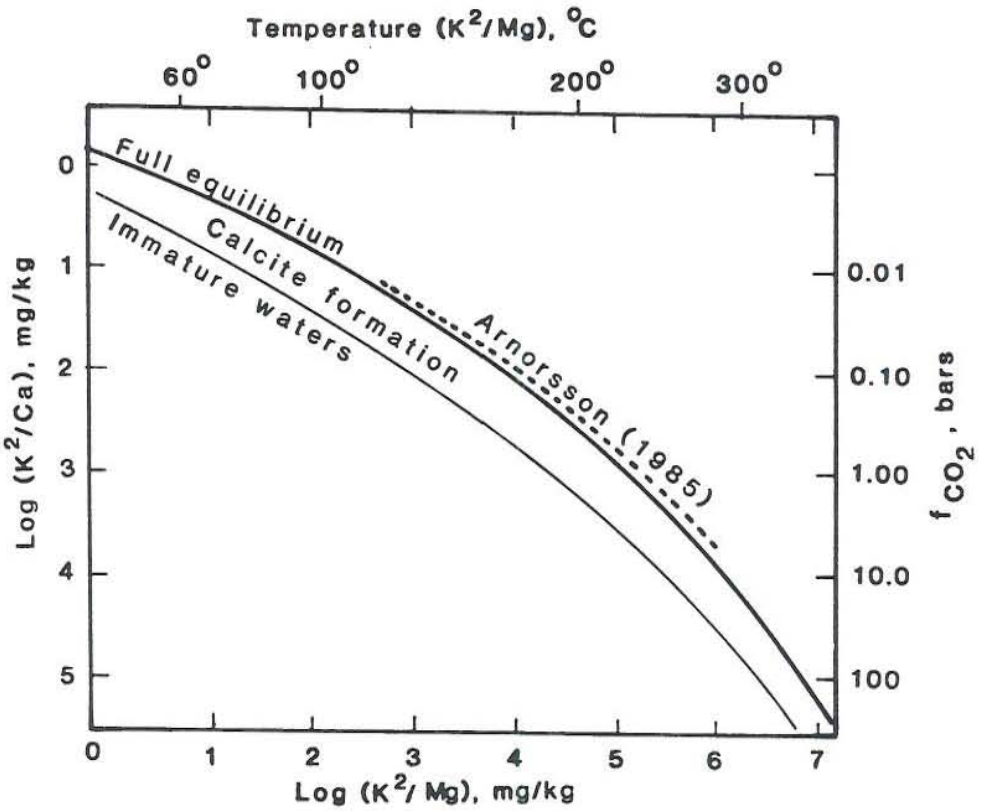

FIGURE 3. Diagram for evaluating K/√Mg and K/√Ca relations in natural waters and for estimating CO_2 fugacities (from Giggenbach, 1988). See text for discussion.

Figure 3 provides a quick means of estimating the partial pressure of CO_2 in a reservoir fluid that is fully equilibrated with the surrounding rock and the pH is controlled by feldspar-mica hydrolysis reactions. Figure 3 cannot be used to obtain the partial pressure of CO_2 in a deep reservoir of relatively acid water, or when an upflowing water has picked up Mg by reaction with the wall rock or by mixing, or when $CaCO_3$ has precipitated as a result of boiling. On the other hand, Figure 3 may be very useful in calling attention to such "problem" waters that do not plot on the fully equilibrated line.

Another use of Figure 3 is for estimating the partial pressure of CO_2 in a geothermal water when the reservoir temperature is known (by measurement in a well or by any given geothermometer) or, conversely, for estimating the reservoir temperature when the partial pressure of CO_2 is known. It is of interest to note that the empirically derived CO_2 geothermometer of Arnorsson (1985) lies very close to the full equilibrium curve of Giggenbach (1988).

CONCLUSIONS

In evaluating cation geothermometer temperatures, attention must be given to possible effects of continuing water-rock reactions and mixing of different waters during upflow. In addition, variations in estimated cation geothermometer temperatures may result from variations in the mineralogy of the reservoir rocks that are reacting with the fluid. Acid conditions at depth may be particularly troublesome and overlooked as a possible source of error when dealing with relatively dilute waters that contain mostly $NaHCO_3$. Additional errors arise from not taking into account activity coefficients of both the solid and ionic reactants. Under the best of conditions cation geothermometers have an uncertainty of at least ± 5-10°C, and commonly much greater than 20°C.

Even with their inherent uncertainties, cation geothermometers can be very useful for estimating approximate temperatures in geothermal systems and for investigating effects of partial water-rock reequilibration during upflow. Reactions involving Na and K appear to proceed very slowly while those involving Mg appear to proceed relatively quickly. In this regard, the salinity of a solution is an important factor because a given amount of reaction of highly saline fluid with wall rock during upflow will have little effect on the ratios of the major cations in solution. On the other hand, the same amount of reaction of a dilute solution with wall rock may drastically change cation ratios. Therefore, cation geothermometry applied to hot-spring waters is likely to be most reliable for highly saline waters and least reliable for dilute water. Increasing Mg, in general, and $K/\sqrt{Mg}$ and $Li/\sqrt{Mg}$, in particular, are very sensitive indicators of water-rock reequilibration with decreasing temperature and of mixing of high- and low-temperature waters.

REFERENCES

Arnorsson, S., 1982, The chemistry of geothermal waters in Iceland. I. Calculation of aqueous speciation from 0° to 370°C: Geochim. Cosmochim. Acta, 46, 1513-1532.

Arnorsson, S., 1983, Chemical equilibria in Icelandic geothermal systems--Implications for chemical geothermometry investigations: Geothermics, 12, 119-128.

Arnorsson, S., 1985, Gas pressure in geothermal systems: Chem. Geol. 49, 319-328.

Fouillac, C. and Michard, G., 1981, Sodium/lithium ratios in water applied to geothermometry of geothermal reservoirs: Geothermics, 10, 55-70.

Fournier, R.O., 1979, A revised equation for the Na/K geothermometer: Geotherm. Resourc. Counc. Trans., 3, 221-224.

Fournier, R.O., and Potter, R.W., II, 1979, Magnesium correction to the Na-K-Ca chemical geothermometer: Geochim. Cosmochim. Acta, 43, 1543-1550.

Fournier, R.O. and Truesdell, A.H., 1973, An empirical Na-K-Ca geothermometer for natural waters: Geochim. Cosmochim. Acta, 37, 515-525.

Giggenbach, W.F., 1988, Geothermal solute equilibria. Derivation of Na-K-Mg-Ca geoindicators: Geochim. Cosmochim. Acta, 52, 2749-2765.

Kharaka, Y.K., Lico, M.S. and Law, L.M., 1982, Chemical geothermometers applied to formation waters, Gulf of Mexico and California basins (abs.): Am. Assoc. Petrol. Geol. Bull., 66, 588.

Kharaka, Y.K. and Mariner, R.H., 1988, Chemical geothermometers and their application to formation waters from sedimentary basins, in Naeser, N.D. and McCollon, T.H. (eds.), Thermal History of Sedimentary Basins, Springer-Verlag, New York, pp. 99-117.

Nieva, D. and Nieva, R., 1987, Developments in geothermal energy in Mexico, part 12--A cationic composition geothermometer for prospection of geothermal resources: Heat Recovery Systems and CHP, 7, 243-258.

Paces, T., 1975, A systematic deviation from Na-K-Ca geothermometer below 75°C and above 10^{-4} atm P_{CO2}: Geochim. Cosmochim. Acta, 39, 541-544.

Tonani, F., 1980, Some remarks on the application of geochemical techniques in geothermal exploration, in Proc. Adv. Eur. Geoth. Res., Second Symp., Strasbourg, pp. 428-443.

Truesdell, A.H., 1976, Summary of section III geochemical techniques in exploration, in Proc. Second United Nations Symposium on the Development and Use of Geothermal Resources, San Francisco, 1975, v. 1: Washington, D.C., U.S. Government Printing Office, pp. 1iii-1xxxix.

DOUBLE-DIFFUSIVE CONVECTION AS A MECHANISM FOR TRANSFERRING HEAT WHILE MAINTAINING CHEMICAL GRADIENTS IN THE SALTON SEA BRINE

Robert O. Fournier
U.S. Geological Survey, Menlo Park, California 94025 U.S.A.

INTRODUCTION

Helgeson (1968) noted that the salinity of the brine in the geothermal reservoir within the Salton Sea geothermal system generally increases from the top to the bottom and from the center to the sides. He also noted that pressure measurements at perforations in cased wells seemed to indicate that the formation fluids at the depths of production all have a specific density about equal to 1, and that hot concentrated brines apparently exist in pressure equilibrium with comparatively cold dilute pore waters in the surrounding rocks. Since 1968 there have been no published reports that dispute these observations. However, a very high heat flux through the top of the system seems to require a substantial component of convective transfer of heat beneath an impermeable cap, whereas the apparent salinity gradient with depth seems to require little or no free convection of brine. This paradox may be resolved if double-diffusive convection is the main process that controls the depth-temperature-salinity relations. Such convection provides a mechanism for transfering heat from the bottom to the top of the hydrothermal system while maintaining vertical and horizontal salinity gradients such that fluid densities remain close to unity everywhere in the reservoir.

DOUBLE-DIFFUSIVE CONVECTION

The processes involved in double-diffusive convection have been reviewed by Huppert and Sparks (1984) and Vitagliano et al. (1984). Double-diffusive convection resulting in layered cells generally has been applied to explain chemical and thermal variations in liquid systems, such

as temperature-salinity profiles in ocean water beneath melting ice (Huppert and Turner, 1981), and to account for stratified chemical variations in some magma chambers (Huppert and Turner, 1981; Huppert and Sparks, 1984). Griffiths (1981) demonstrated experimentally that layered double-diffusive convection cells can form in porous media, and suggested that some chemical variations at Wairakei may be due to this effect.

The two requirements for the occurrence of double-diffusive convection are that the fluid contain two or more components with different molecular diffusivities and that these components make opposing contributions to the vertical density gradient (Huppert and Turner, 1981). In natural hydrothermal systems the important parameters are the contrasting rates of transport of heat and salt across a boundary layer separating cooler less saline water above from hotter more saline water below. Both heat and salt are transported through the interface solely by molecular diffusion.

Thermal input from below into the deeper more saline water causes it to become less dense than the overlying less saline water and convection is initiated. Upward movement of the more saline water continues until a slight cooling increases its density to the point where buoyancy is no longer a driving force. Huppert and Turner (1981) describe the process as follows: "After the initial oscillatory instability, the thermal boundary layer breaks down to form a shallow convecting layer that grows by incorporating fluid from the gradient region above it. When the thermal boundary layer ahead of the convecting region reaches a critical Rayleigh number, it too becomes unstable, and a second layer forms above the first. Convection is sustained by a more rapid vertical transport of heat relative to salt, and eventually many such layers form." For the situation in which there are horizontal as well as vertical temperature and salinity gradients, individual double-diffusive convection cells should be bounded on the sides by other convection cells that have slightly different salinities and temperatures.

APPLICATION TO THE SALTON SEA SYSTEM

Temperature-Depth Profile for Double-Diffusive Convection

Within the Salton Sea hydrothermal system convective flow of fluids appears to be mainly within relatively permeable sands at shallower depths

and mainly within interconnecting fractures deeper in the system where rock has been indurated by metamorphic processes. In response to double-diffusive processes in these porous and fractured environments, temperatures of the wall rocks must adjust to the temperatures of the many-layered convection cells. The measured thermal gradients in wells in the central part of the field generally are nearly linear from the surface to a depth of about 0.5 to 1 km and range from about 250° to 380°C km^{-1}. Below about 1 km, thermal gradients generally are nearly linear, but at much lower values (commonly about 40°C km^{-1}). However, it is likely that the thermal gradient below about 1 km is relatively uniform at about 40°C km^{-1} only on a gross scale, while on a fine scale the thermal profile would have a staircase structure (Figure 1). The size of individual steps in Figure 1 may vary considerably from place to place and change with time. I suspect that most steps are less than a few centimeters to a few meters in height.

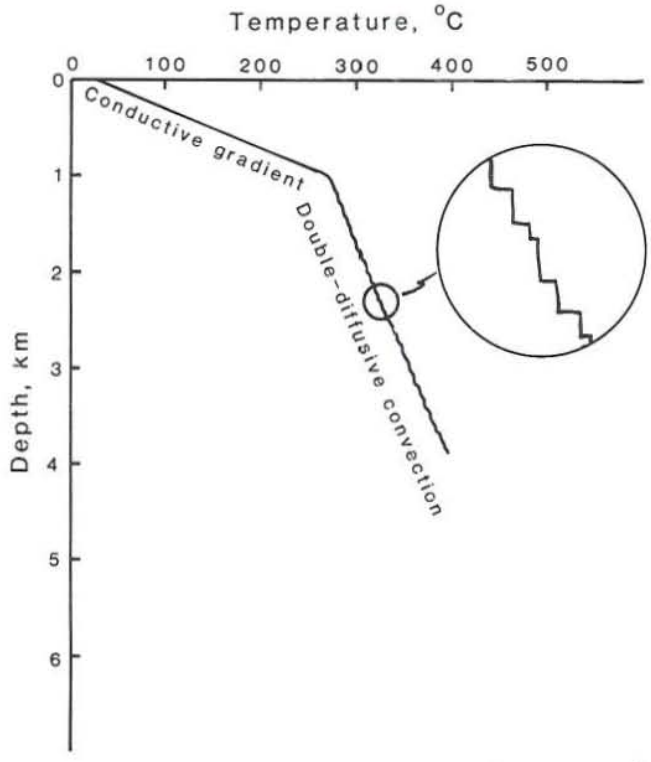

FIGURE 1. Idealized temperature-depth profile within the Salton Sea geothermal system showing details of effects of double-diffusive convection.

Calculation of the Density of a Fluid Sample from the Salton Sea Reservoir

It was previously noted that in order for double-diffusive convection to operate as a mechanism for controlling chemical and thermal gradients within a geothermal reservoir, fluid densities must everywhere adjust to a value about equal to unity. The recently drilled Salton Sea Scientific Drill Hole (SSSDH) provided an opportunity to investigate hydrothermal processes and fluid properties to a depth of over 3 km. An uncontaminated fluid sample was obtained from a depth interval of 1865-1877 m and an initial temperature of 305°C (Michels, 1986; Thompson and Fournier, 1988). The calculated pre-flashed composition of that fluid is shown in Table 1. Although the results provide information about only one point on the depth-composition curve, that point is well constrained, and it can be used to determine whether the fluid density really is close to unity, as it should be if double-diffusive convection is a major process that occurs there.

TABLE 1. Pre-flashed concentrations of selected elements and total dissolved solids in brine from a depth of 1865-1877 m in the State 2-14 well, December 1985 flow test.

Weight %	Dec. 29*	Dec. 29**	Dec. 30**
Na	5.01	5.28	5.27
K	1.72	1.67	1.65
Ca	3.32	2.71	2.65
Cl	15.15	15.34	15.37
Sum	25.20	25.00	24.94
Total dissolved solids	25.2-25.7	25.54	25.46

* Thompson and Fournier (1988)
** Michels (1986)

During drilling, the mud weight required to just balance the pore-fluid pressure at a depth of 1879 m indicated a pore fluid density very close to 1 g cm^{-3}. No downhole-pressure measurements were made at that depth, and downhole-fluid sampling was unsuccessful. Consequently, the only available check on the pore-fluid density is by calculation, using the composition of the brine sampled at the surface corrected for flashing (Table 1). The fluid produced from a depth of about 1870 m is composed predominantly of NaCl, $CaCl_2$, and KCl, and the total dissolved solids are about 25.5 $\pm$ 0.3 weight percent. For this type of brine, the density at high temperature and high pressure can be calculated by using a model published by Potter and Haas (1978). In that model the density of the brine, d_b, is related to the composition of the brine as follows:

$$d_b = d_N + (d_K - d_N)f_K + (d_C - d_N)f_C \ , \qquad (1)$$

where d_N, d_K, and d_C are the densities of pure solutions of NaCl, KCl, and $CaCl_2$, respectively, at the given temperature and molality of the total chloride in solution; and f_K and f_C are the mole fractions of chloride present in the brine as KCl and $CaCl_2$, respectively. Densities of the pure chloride solutions of the three salts were taken from Potter and Brown (1976, 1977) and Potter and Clynne (1976). Density data for KCl at temperatures in the 200° to 400°C range extend only to about 4-m solutions, so densities of a more concentrated solution ranging from 4.0 to 5.8 m were obtained by extrapolation, using a plot of molality chloride versus the difference in density of KCl and NaCl for solutions of the same molality in respect to chloride. That plot and a similar plot with $CaCl_2$ instead of KCl give straight lines (Figure 2). Density data for both KCl and $CaCl_2$ are available only at the vapor pressures of the solutions, and density data for $CaCl_2$ are not available above 300°C. Therefore, densities of the predominantly NaCl-$CaCl_2$-KCl pre-flashed reservoir fluid were calculated at 300°C and the vapor pressure of the solution, and then those results were multiplied by factors to correct for the slightly increased temperature and pressure actually present in the reservoir. The correction factors were obtained by assuming that the changes in density caused by increased temperature and pressure were proportional to the changes in density caused by similar increases in temperature and pressure

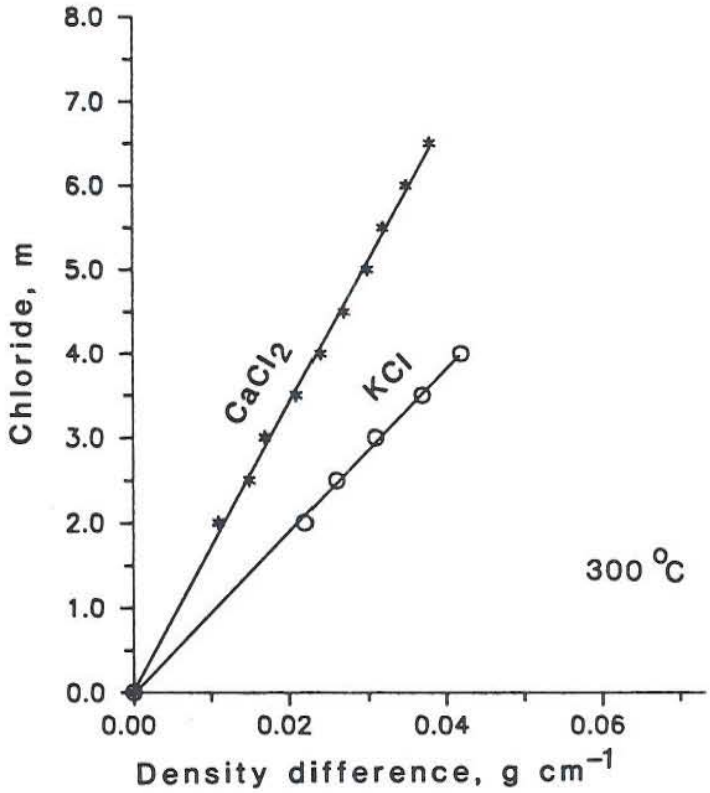

FIGURE 2. Chloride molality versus the density difference between the indicated salt and NaCl at 300°C. The symbols show data obtained from tables of densities.

in the pure NaCl system. The temperature-correction factor that was used required multiplication of the density (calculated at 300°C) and the vapor pressure of the solution by 0.995. The pressure-correction factor required multiplication by 1.019. These corrections for temperature and pressure act in opposite directions, and the combined correction factor requires multiplication by 1.014. The exclusion of iron and other dissolved constituents from the density model is not likely to have made a significant difference, even though they constitute about 2 weight percent of the total dissolved solids, because the model is based mainly on the total chloride in the system. In the Thompson and Fournier data shown in Table 1, all the anionic charges were assumed to be balanced by sodium, calcium, and potassium, thereby compensating in great part for the absence of other dissolved constituents in the density calculation.

TABLE 2. Calculation of specific density of pre-flashed brine at 305°C at a depth of 1865-1877 m in the State 2-14 well. (The notation is given in the text.)

	Dec. 29*	Dec. 29**	Dec. 30**
$d_K - d_N$	0.0604	0.0603	0.0602
$d_C - d_N$	0.0336	0.335	0.335
f_K	0.1029	0.0987	0.0973
f_C	0.3877	0.3125	0.3050
d_{Na}	0.9702	0.9698	0.9696
$(d_K - d_N)f_K$	0.0062	0.0058	0.0059
$(d_C - d_N)f_C$	0.0130	0.0105	0.0102
Sum	0.9894	0.9861	0.9857
P-T correction	x 1.0139	x 1.0139	x 1.0139
Density at 305°C	1.0031	0.9998	0.9994

* Thompson and Fournier (1988)
** Michels (1986)

Calculated densities of pre-flashed reservoir fluids produced from the SSSDH at a depth of 1865-1877 m and a temperature of 305°C are shown in Table 2. The three different sets of analytical information yield a calculated average density of 1.0008 $\pm$ 0.0023. This result is in excellent agreement with a double-diffusive model in which hot brines are in approximate pressure equilibrium with cold water at the sides of the hydrothermal system. The errors caused by not taking account of small amounts of other constituents in the brines, such as iron and manganese, and assuming a model based on pure NaCl to correct for pressures greater than the vapor pressure of the solution and a temperature of 305°C instead of 300°C, will cause the calculated density to be slightly on the low side. Therefore, the chemical data favor reservoir fluid densities of about 1 g cm^{-3} or greater at a depth of 1870 m, which precludes isochemical free convection of fluid from deep in the system to a shallow level. For isochemical conditions in a freely convecting system, brine of the composition found

at 1.8 km would have a density of about 1.02 to 1.03 g cm^{-3} at a depth of 1 km and a temperature of 275°C. That high a fluid density in the shallow part of the system is not consistent with the observed pressures or with free convection driven by the influx of cold dilute water at the sides of the system.

CONCLUSIONS

Double-diffusive convection nicely explains high thermal gradients within the cap of the Salton Sea hydrothermal system (and corresponding large flux of thermal energy) that seems to require convective upflow of thermal energy within the reservoir, while at the same time maintaining vertical and horizontal salinity gradients. The calculated density of the brine sampled from the SSSDH at a depth of 1865-1877 m is close to unity at 305°C and 18.7 MPa. This result is in agreement with a hydrologic model in which hot brines are in hydrostatic equilibrium with cold dilute water surrounding the hydrothermal system. It also is in agreement with a model in which salinity gradients and heat flux are controlled by double-diffusive convection within the hydrothermal system. A depth-temperature-salinity profile in which specific densities of fluids are everywhere close to unity does not in itself prove that double-diffusive convection is occurring. However, double-diffusive convection has been demonstrated experimentally in porous media [Griffiths, 1981], and it should be given additional consideration as a mechanism for explaining the vertical and horizontal chemical gradients and the high heat flux from the Salton Sea geothermal system and other geothermal systems where variations in salinity are found from well to well and at different depths.

REFERENCES

Griffiths, R.W., 1981, Layered double-diffusive convection in porous media: J. Fluid Mech., 102, 221-248.

Helgeson, H.C., 1968, Geologic and thermodynamic characteristics of the Salton Sea geothermal system: Am. J. Sci., 266, 129-166.

Huppert, H.E. and Sparks, R.S.J., 1984, Double-diffusive convection due to crystallization in magmas: Ann. Rev. Earth Planet. Sci., 12, 11-37.

Huppert, H.E. and Turner, J.S., 1981, Double-diffusive convection: J. Fluid Mech., 106, 299-329.

Michels, D.E., 1986, SSSDP fluid compositions at first flow test of State 2-14: Geotherm. Resourc. Counc. Trans., 10, 461-465.

Potter, R.W., II and Brown, D.L., 1976, The volumetric properties of vapor-saturated aqueous potassium chloride solutions from 0° to 400°C based on a regression of the available data: US Geol. Surv. Open-File Rept. 76-243, 5 pp.

Potter, R.W., II and Brown, D.L., 1977, The volumetric properties of aqueous sodium chloride solutions from 0° to 500°C at pressures up to 2000 bars based on a regression of the available data: US Geol. Surv. Bull. 1421-C, 36 pp.

Potter, R.W., II and Clynne, M.A., 1976, The volumetric properties of vapor-saturated aqueous calcium chloride solutions from 0° to 300°C based on a regression of the available data: US Geol. Surv. Open-File Rept. 76-365, 5 pp.

Potter, R.W., II and Haas, J.L., 1978, Models for calculating density and vapor pressure of geothermal brines: J. Res. US Geol. Surv., 6, 247-257.

Thompson, J.M. and Fournier, R.O., 1988, Chemistry and geothermometry of brine produced from the Salton Sea Scientific Drill Hole, Imperial Valley, California: J. Geophys. Res., 95, 13165-13173.

Vitagliano, P.L., Della Volpe, C. and Vitagliano, V., 1984, Gravitational instabilities in free diffusion boundaries: J. Solution Chem., 13, 549-562.

WATER-MAGMA INTERACTION RELATED TO EPISODIC INFLATION AND DEFLATION OF THE YELLOWSTONE CALDERA, WYOMING

Robert O. Fournier
U.S. Geological Survey, Menlo Park, California 94025 U.S.A.

INTRODUCTION

In most current models of magmatic-hydrothermal systems relatively dilute meteoric water circulates along fractures above and to the sides of the magmatic heat source. The maximum temperature attained by the meteoric water is about 350-400°C, and this water is separated from very hot crystalline rock or magma by an impermeable zone where mineral deposition and plastic flow of rock maintains low permeability. Heat extracted by the circulating water slowly cools the system, allowing thermal cracking and faulting to progress inward so that water steadily migrates deeper into the heat source while attaining about the same maximum temperature (Fig. 1). This extraction of heat causes volumetric changes that are relatively small if all the heat is provided by cooling already crystalline rock. In contrast, if some or all of the heat comes from the latent heat of crystallization of magma, the volumetric changes may be relatively large, depending on the amount and rate of magma crystallization, the amount and composition of magmatic fluid liberated, and whether or not that magmatic fluid becomes trapped at lithostatic pressure.

Raised and submerged shoreline terraces of Yellowstone Lake show that there has been episodic uplift interspersed with local deflation of the caldera throughout the Holocene (Hamilton, 1985; Meyer and Lock, 1986), and leveling surveys during the interval 1923-1987 (Dzurisin and Yamashita, 1987 and references therein) showed uplift followed by subsidence. Furthermore, horizontal strain rates measured in the northeastern part of the caldera and in the Hebgen Lake region to the northwest of the caldera appear to preclude regional tectonism as a primary cause of the inflation and deflation. Therefore, at this time it appears that the inflation and deflation are the result of magmatic activity. This paper will summarize possible end-member models that may account for the heat flux from the system and the inflation and deflation of the caldera. More detailed discussions can be found in Fournier and Pitt (1985) and Fournier (1989).

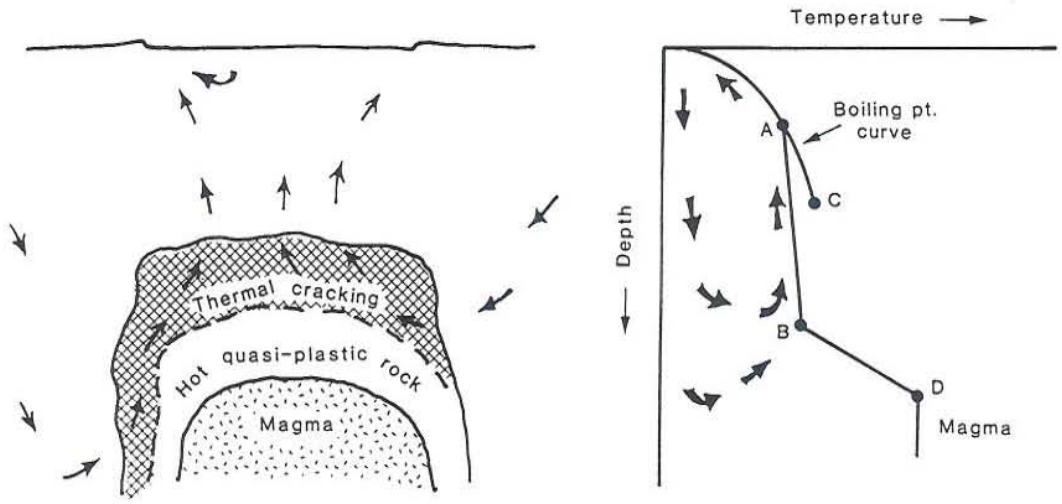

FIGURE 1. Schematic diagram showing circulation of meteoric water extracting heat from a crystallizing and cooling body of magma. There is conductive cooling in the hot quasi-plastic region (D to B) and convective upflow without boiling from B to A. Point C is the critical point of water. The maximum temperature attained by the convecting fluid at hydrostatic pressure is likely to be about 350-400°C.

GEOTHERMAL HEAT FLUX AND DEPTH OF METEORIC WATER CIRCULATION

The water deep in the Yellowstone hydrothermal system contains about 400 mg kg^{-1} Cl before decompressional boiling and before near-surface mixing, and it attains a maximum temperature of about 350°C. This information allows measured rates of discharge of the rivers that drain the Park and of the chloride carried by those river waters to be used to calculate the rate of total discharge of the deep component of the hot-spring water (10^{11} kg yr^{-1}) and its associated heat (4×10^{16} cal yr^{-1} or 5.3×10^{9} W). The river chloride inventory method automatically compensates for boiling and mixing of thermal waters as they rise. Corrections are required, however, for background chloride contributed to the rivers by precipitated rain and snow and by low-temperature weathering of rock. The background Cl generally amounts to about 1-2 mg kg^{-1} in the nonthermal component of the river water, depending on the proportion of water from different nonthermal sources. Note that the river chloride inventory

method generally will give a minimum value for the total heat extracted from the system because it does not take account of heat transferred purely by conduction or of heat transferred convectively by fluids that do not discharge into rivers.

Sustained circulation of hydrothermal fluids at temperatures above about 350-400°C is likely to take place only where rocks are subjected to repeated brittle fracture that counteracts the processes that decrease permeability, precipitation of minerals and quasi-plastic flow of rock that deforms under the force exerted by its weight. Focal depths of well-located earthquakes are deeper than 15 km outside the Yellowstone caldera, but within the caldera they seldom exceed 4-5 km. Evidently the rocks below 3-4 km are too weak as a result of high temperatures (>350°C) to sustain sufficient differential stress for seismic activity to occur (Fournier and Pitt, 1985). Therefore, the maximum depth of sustained fluid flow at hydrostatic pressure is probably about 4-5 km within the caldera and deeper at the sides.

If the assumption is made that thermal energy is transferred uniformly by conduction from the heat source across a 2500-km^2 surface, through hot dry rock to the base of circulation of the hydrothermal system, a thermal gradient of about 700° to 1000°C km^{-1} is required to sustain the average convective thermal output. To account for both the large convective heat flux and the lack of earthquakes below about 4-5 km, it is likely that magmatic temperatures are attained beneath some portions of the caldera at depths as shallow as about 4.5-5.5 km, about the same depth range indicated by various geophysical methods.

CRYSTALLIZATION OF MAGMA AS A SOURCE OF HEAT AND AQUEOUS FLUIDS

If the heat carried in the advective flow of water from the system were supplied entirely by the latent heat of crystallization of rhyolitic magma, about 5×10^{11} kg yr^{-1} of magma (about 0.2 km^3 yr^{-1}) would be required to furnish that heat. In contrast, cooling already crystalline rock by 300°C (to reduce the temperature from about 730° to 430°C) will furnish about the same amount of heat that can be obtained from the latent heat of crystallization of the same volume of rhyolitic magma (using a latent heat of crystallization of 75 cal g^{-1} and heat capacity of 0.25 cal g^{-1}°C). Thus,

crystallizing about 0.1 km^3 of rhyolitic magma and then cooling it about 300°C could furnish the heat carried to the surface by the hot-spring system. A lack of water-bearing minerals in the rhyolite erupted at Yellowstone coupled with the presence of the mineral fayalite suggests that the initial magma contained not more than 1 to 2 weight percent dissolved water. The chloride contained in fresh obsidian glass shows that the minimum initial chloride concentration in the magma was 1500 mg kg^{-1}, and strong partitioning of this chloride into an aqueous magmatic fluid that separates upon slow crystallization of the magma will produce a fluid containing a minimum of 12 to 25 weight percent salt. If the depth of crystallization is about 5 km or less, the evolved magmatic fluid will dissociate into a more highly saline brine containing >50-70 weight percent dissolved salt and an aqueous-rich gas phase containing only about 0.2-2.0 weight percent dissolved salt (Fournier, 1987). The maximum quantity of water that could be liberated by crystallizing 0.2 km^3 yr^{-1} of magma initially containing 2 weight percent water is 8.8×10^9 kg yr^{-1}, and a minimum of about 7×10^8 kg yr^{-1} of chloride would be liberated with that water. For comparison, about 10^{11} kg yr^{-1} water (not including water incorporated by near-surface dilution) and 4×10^7 kg yr^{-1} chloride are discharged by the hot-spring system. Thus, a maximum of about 9 weight percent of the deep component of hot-spring water could be magmatic, but only about 6 weight percent of the available chloride can be discharged with that water. The deficiency of chloride in the thermal water may be interpreted in two ways: (1) Thermal energy is supplied mainly by cooling already crystalline rock with little thermal input from the latent heat of crystallization of magma; or (2) brine evolved from presently crystallizing magma is ponding beneath the dilute hydrothermal system, and only the relatively dilute gaseous component of the aqueous magmatic fluid is incorporated into the convecting meteoric system. Stable isotope data suggest that very little, if any, magmatic water is discharged by the hot springs (Craig et al., 1956; Truesdell et al., 1977). The preferred model is one in which the thermal energy carried to the surface by the convecting hot-spring water comes in part from crystallizing magma and in part from cooling crystalline rock, and that relatively dense brine liberated from the crystallizing magma is accumulating at depth beneath dilute, much less dense hydrothermal waters.

VOLUMETRIC CHANGES ASSOCIATED WITH CRYSTALLIZATION OF MAGMA

Cooling of hot but already crystalline rock should lead to thermal contraction and a subsidence of the caldera floor. However, a significant uplift of the caldera has been measured over the period 1923–1984 (Dzurisin and Yamashita 1987). This inflation stopped in 1985 and deflation occurred in 1986 and 1987. In the eastern part of the caldera, the average vertical velocities of uplift (positive values) and subsidence (negative values) for specific intervals are given in Table 1.

TABLE 1

Year	Vertical Velocity
1923–1976	15±1 mm/yr
1976–1984	22±1 mm/yr
1984–1985	0±7 mm/yr
1985–1986	−26±7 mm/yr
1986–1987	−38±7 mm/yr

The average rate of volume increase for the entire caldera, estimated using the measured rates of uplift in the interval 1923 to 1984 along traverses in the eastern and western parts of the caldera, is about 0.014 km^3/yr.

Meertens and Levine (1985) have suggested that the uplift is the result of horizontal compressive strain, but this does not appear to agree with focal mechanisms of earthquakes within the caldera and the generally extensional tectonic environment of the region. Also, the average horizontal strain rates measured in the northeastern part of the caldera and in the Hebgen Lake region to the northwest of the caldera from September 1984 to August 1987 appear to preclude regional tectonic movements as a primary cause of the inflation and deflation (unpub. data of J.C. Savage and D. Dzurisin).

A best-fit elastic model of the 1984–1987 vertical and horizontal displacements in the eastern part of the Yellowstone caldera involves depressurization or deflation of a 15-km^2 horizontal tabular body at a depth of 10±5 km (J.C. Savage, pers. commun., 1988). A common phenomenon associated with volcanic eruptions (particularly mafic volcanoes like those in Hawaii and Iceland) is inflation during periods when magma rises and accumulates in a shallow reservoir within a volcanic edifice, and deflation when the reservoir ruptures and some or all of this magma drains away,

usually to the side along a rift zone. A lateral draining mechanism does not work well for viscous, silicic magma that is likely to be present at shallow levels beneath the Yellowstone caldera, and there is little geophysical evidence to support a deflation mechanism relying on lateral flow of basalt.

Two mechanisms that might account for the episodic inflation and deflation each require crystallization of rhyolitic magma in amounts that are compatible with the thermal budget for the magmatic-hydrothermal system. Both mechanisms may operate to varying degrees at the same time.

Episodic Intrusion of Basalt and Continuous Crystallization of Rhyolite

Episodic intrusion of basalt from the mantle into the crust at one level and continuous crystallization of rhyolitic magma at a shallower level can explain the inflation and deflation without the need for a lateral draining of basalt away from the caldera. The thermal energy discharged by advecting thermal waters at Yellowstone is about equal to the latent heat of crystallization of 0.2 km^3/yr of rhyolitic magma (Fournier and Pitt, 1985). If purely conductive heat flow and heat carried upward by convecting hydrothermal fluids that do not discharge at the surface also were taken into account, the amount of magma required to supply the total thermal flux by latent heat of crystallization would be correspondingly higher. Crystallization of 0.2 km^3 of rhyolitic magma would lead to a volumetric contraction of about 0.014 km^3, provided all evolved magmatic gas escaped into the overlying hydrostatically pressured hydrothermal system. Thus, if the latent heat of crystallization of magma is the principal source of thermal energy for the hydrothermal system, and if the evolved magmatic fluids continuously and efficiently escape from the system, the usual state of deformation of the caldera should be deflation at a rate that is close to the observed rate of subsidence since 1985. Inflation would occur only during periods of episodic intrusion of basalt from the mantle into the upper crust (a depth of about 10±5 km) at a rate fast enough to more than compensate for the decrease in volume resulting from crystallizing rhyolitic magma. Stability at the caldera floor would occur only when the volume increase resulting from basalt intrusion (and possibly related melting of silicic material) at the base of the relatively high-level magma chamber just balanced the volume decrease resulting from crystallizing rhyolite at the top of the chamber.

Accumulation of Magmatic Gas at Lithostatic Pressure

A mechanism that can explain both the inflation and deflation of the caldera without any intrusion of basalt into the crust from the mantle involves accumulation of evolving magmatic gas at lithostatic pressure in a deep hydrothermal system and episodic injection of that gas into the overlying hydrostatically pressured system.

Self-sealing at the base of the hydrostatically pressured hydrothermal system is likely to occur as a result of chemical transport and precipitation of vein minerals and ductile flow of rock that becomes relatively weak at temperatures exceeding 400°C. If the magmatic fluid that is liberated during crystallization of 0.2 km^3/yr of rhyolitic magma containing about 2 weight percent water becomes trapped at lithostatic pressure beneath such a self-sealed zone, there will be a net volume increase of about 0.026 km^3/yr, about twice the observed rate of inflation of the caldera from 1923 to 1984. Thus, there is latitude for both crystallization and subsequent partial cooling of rhyolitic material during inflation of the caldera. The calculation of the net volume increase is not particularly sensitive to the initial ratio of water to chloride in the magma because, at the likely depth and temperature of crystallization, the magmatic fluid will dissociate to a small amount of very saline brine plus gas containing 2-3 wt percent dissolved salt. Episodic hydrofracturing and injection of evolved magmatic fluids into the hydrostatically pressured hydrothermal system would result in episodic deflation of the caldera. The pressure surge within the low-pressure portion of the hydrothermal system may be accommodated entirely or in part by an increased rate of flow of thermal water at the surface, by a decrease in the rate of recharge of cold meteoric water into the system, or by condensation of a relatively small amount of steam and slight rise in the level of the interface between liquid and steam within a deep vapor-dominated region that appears to be widespread in the eastern part of the Park. A drop in pressure from lithostatic to hydrostatic at temperatures exceeding 400°C will result in massive precipitation of quartz and other minerals that will tend to heal the break in the self-sealed zone. Thus, the process of inflation and deflation associated with accumulation and escape of high-pressure fluids will become episodic.

Although the above calculations and speculations do not demonstrate conclusively a causal relationship between the uplift and liberation of fluid from crystallizing magma, they do show that the volumetric effects of liberating a magmatic fluid could be important if the latent heat of crystallization of magma is an important source of energy for the hydrothermal system.

CONCLUSIONS

Subsidence is normal within silicic caldera complexes where molten or partly molten material is crystallizing at relatively shallow depths and evolved magmatic fluid escapes from the system. Episodic uplift may result from upward movement of magma (particularly basalt from the mantle into the upper crust) and (or) from accumulation of evolved magmatic gas at lithostatic pressure. The heat discharged by the hydrothermal system at Yellowstone is more than sufficient to explain the subsidence by a magma crystallization mechanism and episodic inflation and subsidence either by pressurization and depressurization of evolved magmatic gas or by episodic intrusion of basalt into the crust from the mantle. Although either of the above mechanisms could eventually culminate in renewed volcanic activity, they are not necessarily indicative of an imminent eruption. However, the eruption hazard cannot be ignored. At this time the most plausible model for the magmatic-hydrothermal system is one in which the thermal energy carried to the surface by the advecting hot-spring water comes in part from crystallizing silicic magma and in part from cooling crystalline rock, and brines are accumulating deep in the system. It is likely that crystallization and cooling are occurring at some levels while new magmas (basaltic and silicic) accumulate at others.

REFERENCES

Craig, H., Boat, G. and White, D.E., 1956, Isotope geochemistry of thermal waters: Natl. Acad. Sci. Natl. Res. Counc. Publ. 400, 29-39.

Dzurisin, D. and Yamashita, K.M., 1987, Vertical surface displacements at Yellowstone caldera, Wyoming, 1976-1985: J. Geophys. Res., 92, 13753-13766.

Fournier, R.O., 1987, Conceptual models of brine evolution in magmatic-hydrothermal systems, in Decker, R.W., Wright, T.L. and Stauffer, P.H. (eds.), Hawaiian Volcanism: US Geol. Surv. Prof. Pap. 1350, pp. 1487-1506

Fournier, R.O., 1989, Geochemistry and dynamics of the Yellowstone National Park hydrothermal system, Wyoming: Ann. Rev. Earth Planet. Sci. (in press).

Fournier, R.O. and Pitt, A.M., 1985, The Yellowstone magmatic-hydrothermal system, in Geothermal Resources Council 1985 International Symposium on Geothermal Energy [transactions], Stone, Claudia (ed.): International Volume, pp. 319-327.

Hamilton, W.L., 1985, Deformation models for interpreting warped Holocene terraces of Yellowstone Lake and the Yellowstone River at the Yellowstone caldera, Wyoming (abs.): Eos Trans. AGU, 66(46), 853.

Meertens, C. and Levine, J, 1985, Compressive tectonic strain as a possible mechanism for long-term vertical deformation of the Yellowstone caldera (abs.): Eos Trans. AGU, 66(46), 853.

Meyer, G.A. and Lock, W.K., 1986, Origin and deformation of Holocene shoreline terraces, Yellowstone Lake, Wyoming: Geology, 14, 699-702.

Truesdell, A.H., Nathenson, M. and Rye, R.O., 1977, The effects of subsurface boiling and dilution on the isotopic compositions of Yellowstone thermal waters: J. Geophys. Res., 82, 3694-3704.